

Sample only

CHAPTER 49

Diseases of the Limbs

KANG Heung Sik, CHO Kil Ho, RYU Kyung Nam

Shoulder	1055
Elbow	1062
Hand and Wrist.....	1069
Hip	1075
Knee	1080
Ankle	1090
References	1095

SHOULDER

The shoulder has a greater range of motion than any other joint in the human body. However, stability of this joint is limited due to a relatively-small and shallow glenoid (socket) compared to the humeral head (ball). Radiologists and clinicians rely on information provided by conventional radiography, arthrography, scintigraphical imaging, CT scanning, CT arthrography, US and MR imaging for evaluation of the shoulder. Radiography plays a fundamental role in the assessment of internal derangements of the shoulder region. With glenohumeral joint arthrography, the width of the rotator cuff and the integrity of cuff tendons, and the glenoid labrum can be assessed. US provides a successful non-invasive approach for examination of

rotator cuff, biceps tendon and muscles. Technical advances such as those related to the design of surface coils have led to a gradual improvement in the quality and diagnostic accuracy of MR examinations of the shoulder [1].

Shoulder impingement syndrome

The impingement syndrome is a clinical entity characterised by a variety of signs and symptoms that result from the restricted space that exists between the coracoacromial arch above and the humeral head and tuberosities below [2]. The tendons of the rotator cuff and the long head of the biceps brachii muscle, as well as the coracohumeral ligament, pass through this space. The causative factors of the impingement syndrome can be divided into two groups, namely: structural factors and functional factors. Structural factors relate to the acromioclavicular (AC) joint, acromion, coracoid

The Asian-Oceanian Textbook of Radiology, 2003.
Edited by Wilfred C.G. Peh & Yoshihiro Hiramatsu.

Sample only

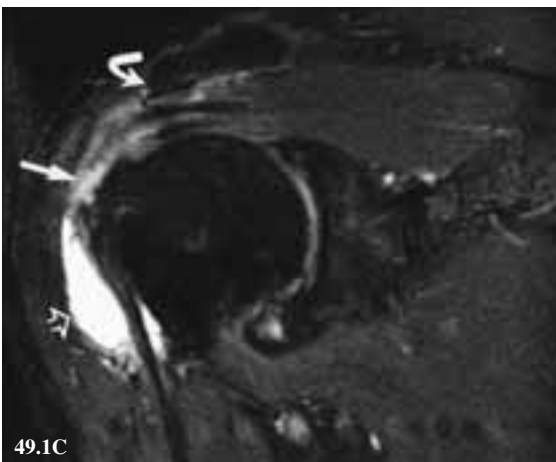
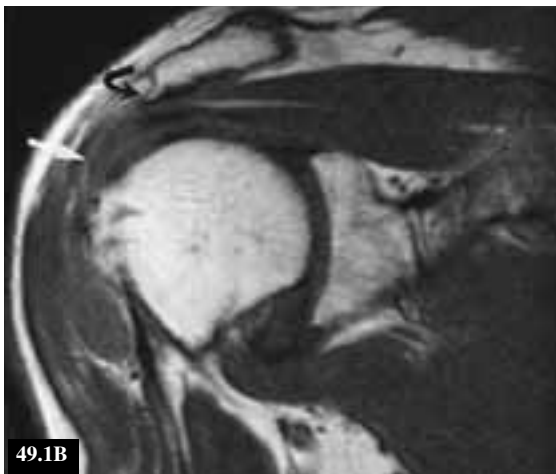


Fig. 49.1: Full-thickness rotator cuff tears with subacromial enthesophyte. (A) Y-view radiograph shows a subacromial enthesophyte (arrow). Oblique coronal (B) T1-W and (C) fat-suppressed T2-W MR images show a tear of the supraspinatus tendon (arrow) which is of hyperintense signal. Fluid (open arrow) in subdeltoid bursa and subacromial enthesophyte (curved arrow) are noted. (D) Oblique sagittal T1-W MR image shows a marrow-containing subacromial enthesophyte (arrow).

process, and humerus. Osseous changes including subacromial enthesophyte (Fig. 49.1), osteophyte of the AC joint, anteriorly-hooked acromion, low-lying acromion, and os acromiale may lead to extrinsic impingement [3].

The value of imaging in the assessment of the shoulder impingement syndrome includes morphological features of the acromion, thickening of the coracoacromial ligament, and the status of the rotator cuff [4,5]. MR imaging allows detection of abnormalities of the rotator cuff, the acromion, the AC joint, and the subacromial bursa. The shape of the acromion can be determined on the oblique sagittal MR images located lateral to the AC joint. Correlations between the hooked acromion and clinical impingement have been reported [3,6]. An anterior acromial enthesophyte, which arises at the acromial attachment site, is a highly specific radiographical manifestation of the shoulder impinge-

ment syndrome [4]. The osteophytes may be apparent on radiographs (Fig. 49.1A) of the shoulder, and are observed on coronal oblique and sagittal oblique MR images (Figs. 49.1B - D) as bony outgrowths. These outgrowths often contain marrow, and extend from the anteroinferior portion of the acromion. Osteophyte and capsular hypertrophy of the AC joint may contribute to the shoulder impingement syndrome, although AC joint arthrosis is not specific for impingement [7]. A thickened coracoacromial ligament (Fig. 49.2) has been found to be associated with the impingement syndrome [8]. The criteria for determining thickening of the ligament on MR imaging are subjective, and no reproducible measurement has been reported [3].

Rotator cuff tears

Ischaemic event (hypovascularity), age-related degeneration of the tendon, and extrinsic factors, including cuff impingement, are proposed causes of

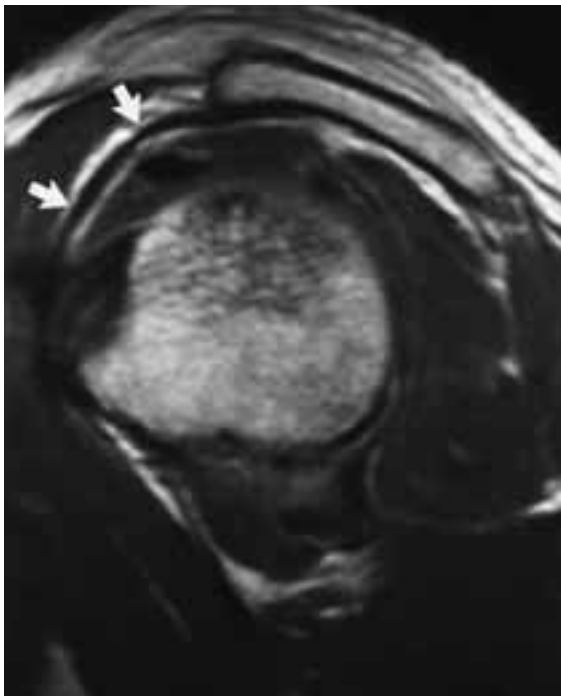
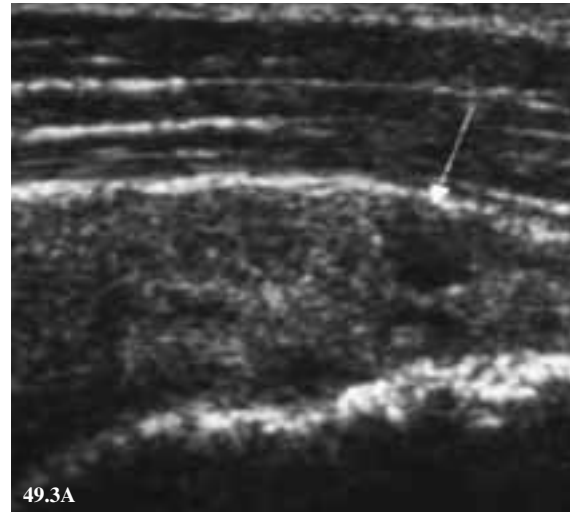


Fig. 49.2: Thickened coracoacromial ligament. Oblique sagittal PD-W MR image shows thickening of the coracoacromial ligament (arrows).



49.3A



49.3B

Fig. 49.3: Rotator cuff tear. US scans taken in the (A) oblique coronal and (B) oblique sagittal planes show a hypoechoic tear (arrows) in the supraspinatus tendon. (HH: humeral head).

rotator cuff tears. The usual “rotator cuff tear” most often refers to a tear of the supraspinatus tendon. Isolated tears of the infraspinatus and subscapularis tendons are uncommon [9]. Radiography, arthrography, US and MR imaging are often applied to the assessment of rotator cuff abnormalities. The value of US in the assessment of the rotator cuff is well established (Fig. 49.3). Conventional arthrography remains a popular technique in the diagnosis of rotator cuff tears. MR imaging is considered superior to US and conventional arthrography in the assessment of rotator cuff tears.

Both the oblique coronal plane, i.e. parallel to the long axis of scapula and roughly parallel to the

long axis of the supraspinatus tendon, and sagittal oblique plane, i.e. perpendicular to the long axis of the scapula, are useful for the evaluation of rotator cuff disorders. The normal tendons of the rotator cuff have a hypointense signal on all MR imaging sequences, contrasting with areas of hyperintense signal in abnormal tendons on some MR imaging sequences. However, much debate and investigation have focused on the cause of increased signal intensity within the supraspinatus tendon [10]. Magic angle phenomenon, partial volume averaging, variations in normal anatomy, and mucoid

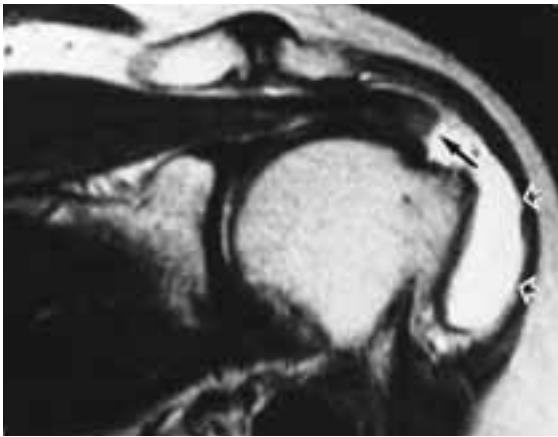


Fig. 49.4: Full-thickness rotator cuff tear. Oblique coronal T2-W MR image show a full-thickness tear of the supraspinatus tendon (arrow) and fluid in the subacromial-subdeltoid bursa (open arrows).

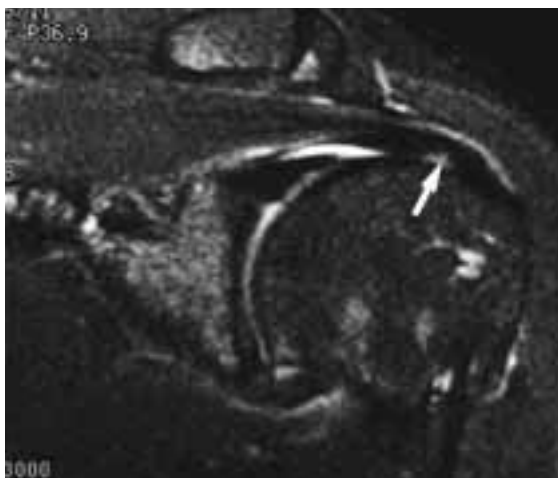


Fig. 49.5: Partial-thickness rotator cuff tear. Enhanced oblique coronal fat-suppressed T1-W MR image shows a region of increased signal intensity (arrow) involving the articular surface of the supraspinatus tendon.

degeneration are some causes of this spurious hyperintense signal. A full-thickness rotator cuff tear involves a complete disruption of the tendon from the articular to the bursal surface. The MR imaging features of full-thickness tears of the rotator cuff include a tendinous defect (Figs. 49.1 & 49.4) that is filled with fluid or granulation tissue, and retraction of the musculotendinous junction beyond the normal limits. Secondary signs of full-thickness tear include fluid in the subacromial-subdeltoid bursa, fluid in the glenohumeral joint, loss of the peribursal fat plane, and muscle atrophy. Fluid in the subacromial-subdeltoid bursa (Fig. 49.4) is a common but relatively non-specific finding in patients with rotator cuff tears. The fluid may be present on the basis of “reactive” subacromial bursitis or may escape from the glenohumeral joint through a tear of the rotator cuff into the bursa. Small amounts of fluid in the bursa can be seen as an isolated finding [11].

The detection of partial-thickness tears of the rotator cuff is more difficult than that of full-thickness tears. Partial-thickness tears may involve either the bursal or articular surface of the tendon (Figs. 49.5 & 49.6). Tears of the articular surface are more common than bursal surface partial-thickness tears. A region of increased signal intensity in the superficial portion of the tendon, perpendicular to the long axis of the tendon, on oblique coronal spin-echo T2-weighted images is most consistent with the diagnosis of a partial-thickness tear. Partial-thickness tears of the rotator cuff may be associated with changes in tendon morphology, and are not associated with changes in signal intensity. MR arthrography may increase diagnostic accuracy in patients with articular surface partial-thickness tears of the rotator cuff [1,3] (Fig 49.7).

Experienced observers interpreting carefully-performed MR examinations will provide an accurate diagnosis of a full-thickness tear in more than 90% of patients with such tears. Diagnostic pitfalls

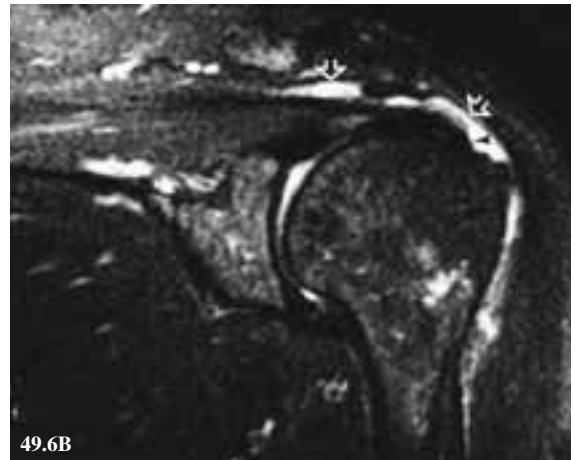


Fig. 49.6: Partial-thickness rotator cuff tear. Oblique coronal (A) T1-W and (B) T2-W MR images show a partial tear (arrowhead) involving the bursal surface of the supraspinatus tendon. Subacromial enthesophyte (short curved arrows) and fluid in the subacromial-subdeltoid bursa (open arrows) are present.

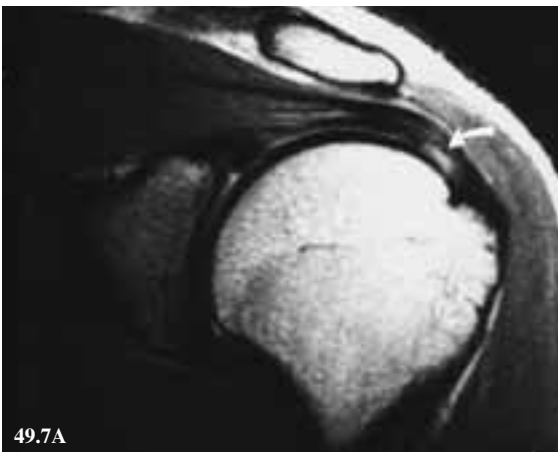


Fig. 49.7: Partial-thickness rotator cuff tear. (A) Oblique coronal PD-W MR image shows a region of hyperintense signal (arrow) at the articular surface of the supraspinatus tendon. (B) Oblique coronal T1-W MR arthrographic image confirms a partial-thickness tear (arrow) of the articular surface of the supraspinatus tendon.

that cause the most difficulty are the normal alterations in signal intensity that occur at the attachment site of the supraspinatus tendon and at the rotator interval, the presence of articular cartilage of the humeral head beneath the distal portion of the supraspinatus tendon, and the occurrence of muscle fibres between the supraspinatus and infraspinatus tendons.

Tendinopathy

The term tendinitis has been used loosely to describe signal intensity alterations in the rotator cuff tendons. The histological findings are more

compatible with an ischaemic or degenerative process than an inflammatory one [12]. A more appropriate term for this process is **tendinopathy** or tendinosis rather than tendinitis [1]. The MR imaging characteristics of rotator cuff tendinopathy or tendinosis include increased signal intensity in a tendon with normal or abnormal morphology (Fig. 49.8) and an intact peribursal fat plane. In general, the signal intensity of the lesion is not as marked as that of a tear on T2-weighted MR images [13].

Common sites of articular and periarticular calcific deposits are the tendinous, capsular, ligamentous, and bursal tissues around the shoulder. The

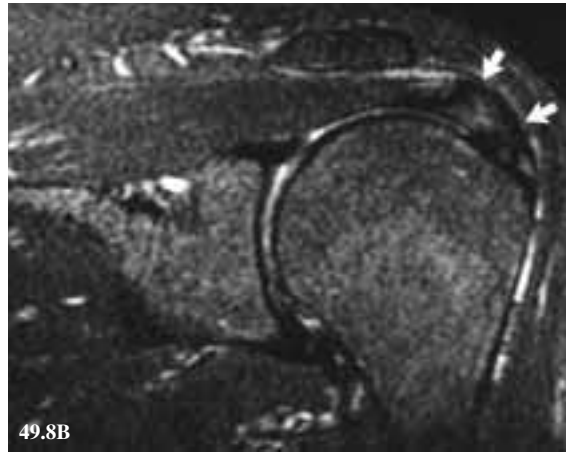


Fig. 49.8: Tendinosis or tendinopathy of the rotator cuff. Oblique coronal (A) T1-W and (B) enhanced fat-suppressed T1-W MR images show contour bulging and increased signal intensity in the distal part of the supraspinatus tendon (arrows).

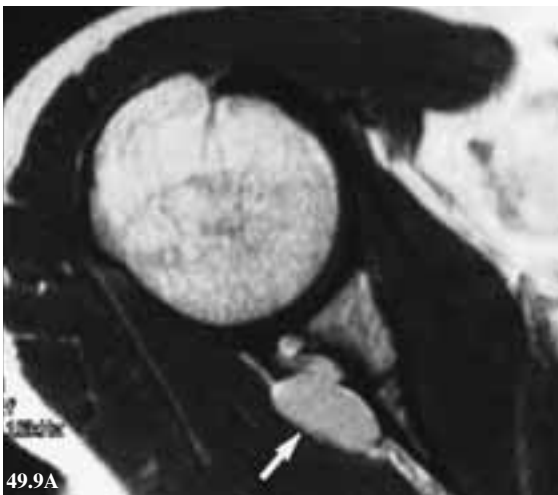


Fig. 49.9: Ganglion cyst. (A) Axial PD-W and (B) coronal T2-W MR images show a ganglion cyst (arrows) in the posterior aspect of the spinoglenoid notch of the scapula. No associated atrophy of the infraspinatus muscle is present.

deposits are frequently asymptomatic although they may produce significant symptoms and signs, including pain, tenderness, swelling, and restricted motion. The pain is caused by inflammation. Calcific tendinitis is most common in the region of the critical zone of the supraspinatus tendon. Calcific tendinitis is diagnosed more easily on radiographs than on MR imaging. The radiographical appearance of calcific tendinitis depends on the location of the abnormal deposition of calcium hydroxyapatite crystals. Intratendinous or intrabursal calcification are seen as hypointense regions on all MR sequences [14].

Synovial abnormalities

A variety of synovial inflammatory disorders, such as rheumatoid arthritis, involve the glenohumeral joint and subacromial-subdeltoid bursa. Radiography has been the mainstay for imaging evaluation of arthritis. Arthrography, bursography, US, CT and MR imaging offer advantages of visualisation of the synovial inflammatory tissue. The synovial lining shows a broad spectrum of involvement in various articular disorders. MR imaging findings of synovitis within the glenohumeral joint or subacromial-subdeltoid bursa include increased amount of synovial fluid, intrasynovial regions of

low signal intensity representing fibrous bodies, synovial cysts, and enhancement of the synovial membrane after the intravenous administration of gadolinium compounds [17]. The presence of haemosiderin deposition or cartilage nodules on MR imaging may be diagnostic in cases of pigmented villonodular synovitis or idiopathic synovial osteochondromatosis.

Entrapment neuropathies

The suprascapular nerve, which contains motor and sensory fibres, may become compressed along its path by masses such as ganglia. The most frequent site of nerve entrapment is at the point where the nerve passes through the suprascapular notch. This entrapment usually occurs in young men, and is common in manual labourers or weightlifters. Ganglia arising at the scapular notch (Fig. 49.9) compress motor branches of the suprascapular nerve, resulting in weakness or atrophy of both the supraspinatus and infraspinatus muscles. Ganglia arising near the spinoglenoid notch affect a more distal segment of the nerve, resulting in selective involvement of the infraspinatus muscle. MR imaging findings include a fluid-filled mass communicating with the joint, muscle atrophy, and rotator cuff tear. Associated tears of the glenoid labrum and posterior portion of the glenohumeral joint capsule also are observed, suggesting that the pathogenesis of some of these ganglion cysts is similar to that of meniscal cysts about the knee [16].

Tumours

Any type of bone and soft tissue tumour can arise around the shoulder. Of the benign bone tumours, osteoid osteoma deserves emphasis owing to its characteristic radiographical and MR imaging features (Fig. 49.10). Intra-articular osteoid osteo-



Fig. 49.10: Osteoid osteoma. (A) AP radiograph shows a small osteolytic lesion (arrow) in the medial aspect of the humeral neck. (B) Axial T1-W and (C) enhanced oblique coronal T1-W MR images show a nidus (arrowhead) and thickened synovium (arrow).

ma can produce marked synovial inflammation. Both benign and malignant cartilage tumours, such as enchondroma and chondrosarcoma, are not uncommon around the shoulder. Osteosarcoma may also occur at this site. Soft tissue tumours, such as desmoid tumours, elastofibroma, lipoma and liposarcoma, and haemangiomas may be encountered around the shoulder [1].

ELBOW

In the elbow, diseases related to chronic overuse are more commonly encountered although the elbow is vulnerable to acute trauma [17,18]. When conventional radiographs, fundamental for initial evaluation of bone disease, are non-diagnostic, several other modalities are available. Scintigraphical imaging is helpful for the early detection of pathological processes, but lacks specificity. Currently, MR imaging is the modality of choice for assessment of all the intra-articular and peri-articular structures. Indications include determining the exact site and severity of pathology, identifying potential concurrent abnormalities, and excluding other causes of pain [19,20]. High-resolution US may also be carried out following clinical and radiographical assessment, not only to demonstrate abnormalities but also to allow transducer compression of these abnormalities to see if the patient's characteristic symptoms are reproduced [21,22]. Lateral elbow pain may be caused by a variety of processes including lateral collateral ligament sprain or tear, focal synovitis, overlying bursi-

tis, and rarely, radial nerve compression or entrapment.

Tendon lesions

Lateral epicondylitis

Lateral epicondylitis, also called "tennis elbow", is one of the most common sources of elbow pain. It is 7 to 10 times more frequent than medial epicondylitis [23]. Lateral epicondylitis rep-

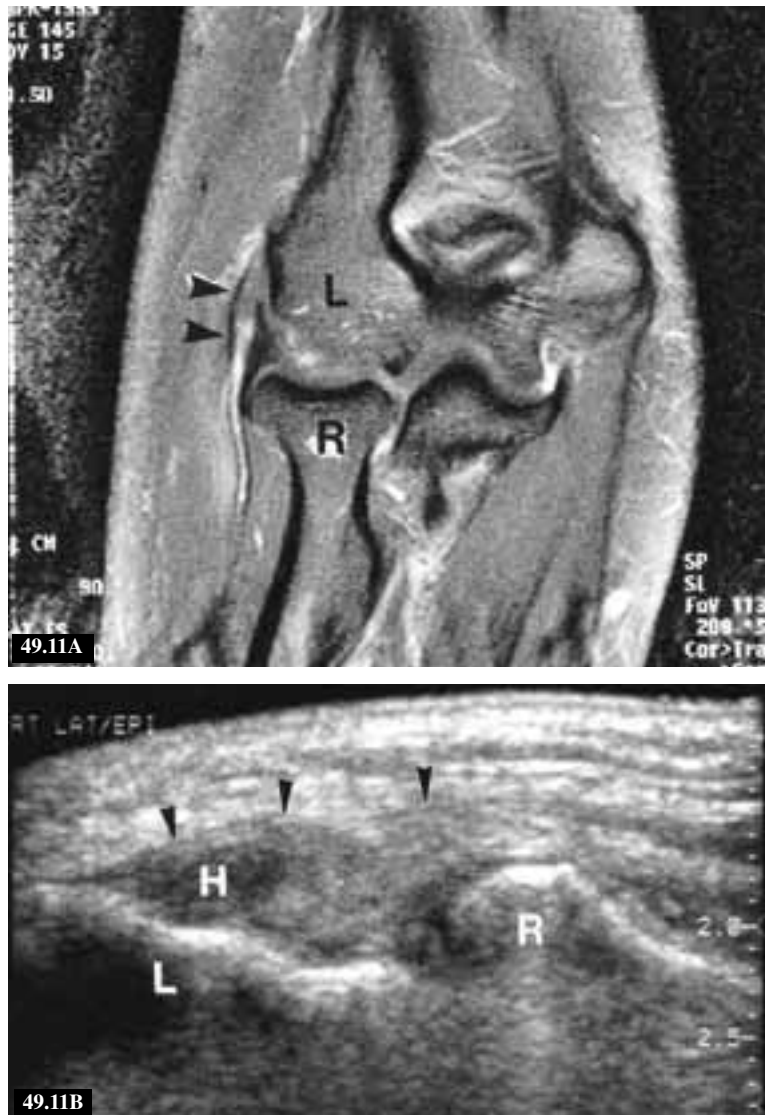


Fig. 49.11: Lateral epicondylitis. (A) Enhanced coronal T1-W MR image shows diffuse thickening of the tendon (arrowheads) of the forearm common extensors. (B) Longitudinal US scan shows diffuse thickening of the tendon (arrowheads) with an intra-tendinous hypoechoic area (H) representing inflammation. (L: lateral epicondyle, R: radial head).

resents a symptom complex with pain and tenderness over the lateral epicondyle at which the common forearm extensors arise. It involves primarily the origin of the extensor carpi radialis brevis muscle, and occasionally, the extensor digitorum communis, and the surface of the extensor carpi radialis longus [25]. Histologically, there is neovascularisation, disruption of collagen, and mucoid degeneration without inflammation, thus confirming that the tendon undergoes a degenerative rather than an inflammatory process [24,25].

Conventional radiographs are abnormal in 20% of patients, with a spur at the epicondyle or tiny calcification in the common extensor tendon [23,26]. These calcifications are more difficult to recognise on MR imaging [19]. MR findings are: hyperintense signal of the tendon, contour change, and fluid around the tendon [18-20,24]. On US, the tendon is thickened with heterogeneous hypoechogenicity, sometimes with calcific foci within the tendon, fluid collection around the tendon-bone junction, and cortical irregularity of the epicondyle [21,27] (Fig. 49.11). In addition, US is helpful to depict minor changes of intra-tendinous fibrillar pattern, and to detect a functional impairment of the tendon by dynamic examination.

Medial epicondylitis

Medial epicondylitis is caused by repetitive valgus stress in the overhead position. A specialised technique used in baseball pitching, for example, leads not only to an injury at the tendon of the common forearm flexors originating from the medial epicondyle, but also to the medial collateral ligament and ulnar nerve. The origins of the pronator teres and flexor carpi radialis muscles are affected in many cases of medial epicondylitis [26]. Imaging findings of medial epicondylitis are similar to those of lateral epicondylitis [20]. “Little League” elbow is a complex injury including medial epicondylitis, lateral impingement, posterior impingement, and

ulnar nerve compression. MR imaging and US of the elbow in cases of epicondylitis are often useful in clarifying the site and degree of injury, especially in a patient who does not respond to conservative treatment, and in the assessment of healing [19-21].

Other tendon injuries

The tear of the distal biceps tendon frequently accompanies an avulsion injury from the radial tuberosity, resulting in classic “popeye” deformity of the retracted muscle belly when a complete tear has occurred [28]. Rupture of the biceps tendon occurs when a sudden hyperextension force is applied to a flexed supinated arm [29,30]. A displaced fracture of the olecranon tip or radial tuberosity may be functionally equivalent to a triceps or biceps tendon rupture. Tear of the triceps tendon occurs at the tendinous insertion onto the olecranon during a fall on a flexed arm, or secondary to forced hyperextension or a direct blow. Both US and MR imaging (using sagittal and axial T2-weighted or STIR images) are useful to depict the tendon tears. Findings include a partial or total absence of the tendon, a fluid-filled tendon sheath, haematoma formation, and muscle oedema [20,21,29,31,32]. Tendinitis is usually manifested by a thickened tendon with hyperintense intra-tendinous signal, with or without peritendinous fluid, on T2-weighted MR images. On US, tendinosis shows similar findings to those seen on MR imaging [21].

Bursitis

Bursal enlargement may result from a variety of diseases, including trauma, rheumatoid arthritis, gout, haemodialysis, diabetes mellitus, and infection. When the bursae are inflamed, MR imaging and US may demonstrate a fluid-filled bursal space within which a variable amount of synovial proliferation and wall thickening are seen

[21,22,33] (Fig. 49.12). The lateral radiograph of the elbow may show an area of soft tissue bulging at the olecranon area. US is usually requested to confirm the bursal enlargement when the clinical examination was not able to distinguish cellulitis, synovitis, or a solid mass from bursitis [21]. MR imaging is very useful for excluding underlying osteomyelitis, arthritis, and to preoperatively determine the extent of the involvement. Enhanced fat-suppressed T1-weighted MR images show a fluid-filled bursal cavity in which its wall has an irregularly-thick enhancing frond-like synovial proliferation.

However, differentiating septic from non-infectious conditions may be difficult by imaging alone, thus aspiration with fluid analysis is mandatory for this purpose in suspected cases [33]. Anteriorly, the interosseous and bicipito-radial bursae, with inter-communications between them, are located at the insertion of the distal biceps tendon on the radial tuberosity. An enlarged bursa at the antecubital fossa may compress the median nerve medially, and posterior inter-osseous branch of the radial nerve laterally, resulting in nerve compression or irritation [34,35]. Differential diagnosis includes

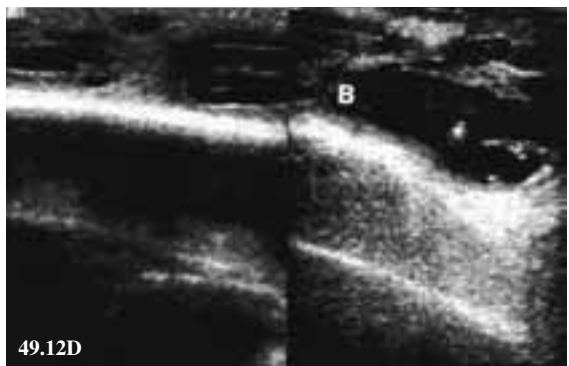
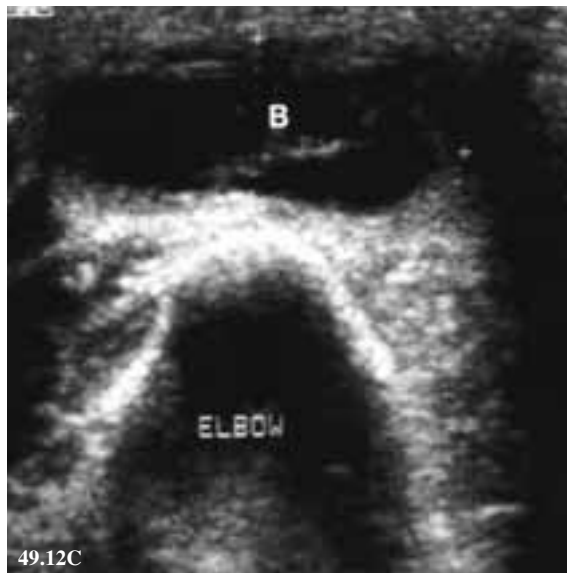
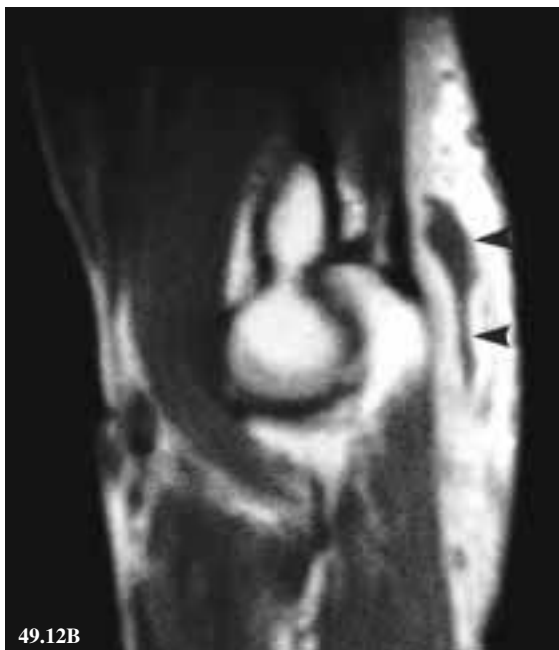
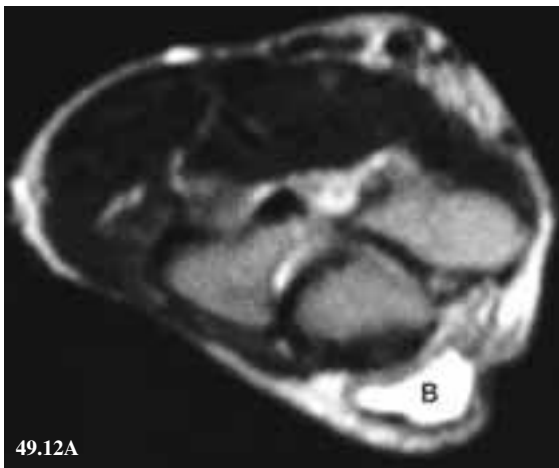


Fig. 49.12: Olecranon bursitis. (A) Axial T2-W MR image shows a hyperintense olecranon bursa (B) within the soft tissues in the posterior aspect of the elbow. (B) Enhanced sagittal T1-W MR image shows peripheral rim enhancement of the bursa (arrowheads). US scans taken in the (C) transverse and (D) longitudinal (composite) planes show synovial proliferation within the bursa (B).

ganglion cyst, solid masses, or vascular malformation [21].

Neuropathies

Three major nerves may be compressed around the elbow. These are: the ulnar nerve posteromedially, the median nerve anteromedially, and the radial nerve anterolaterally. They are located either within anatomically-narrow spaces that are rigid osteofibrous tunnels, or beneath prominent or abnormal band of muscles, connective tissues or bony ridges [36-38]. Nerve compression is produced by direct trauma, tumours, inflammatory processes, and oedema of surrounding soft tissues by a variety of causes [19,20,36-38]. The ulnar nerve is the most frequently-involved nerve because of its superficial location in a relatively fixed state within the cubital tunnel just posterior to the medial epicondyle of the humerus [29].

Potential causes of compression are medial epicondylar fracture, thickened cubital retinaculum, an anomalous anconeus epitrochlearis muscle, osteophyte, or masses such as ganglion cyst, lipoma, and haemangioma within the tunnel [19,20,29,38]. Asymptomatic subluxation of the ulnar nerve may be seen normally [36]. On MR imaging and US, causes of nerve compression may be detected. The nerve is hyperintense with flattening or enlargement on T2-weighted MR images [19,20,36,37]. It may however be difficult or time-consuming to depict a longitudinal image of the nerve on MR imaging. In this situation, high-resolution US is helpful to trace along the course of the nerve to evaluate the internal echo texture of fascicles within the nerve [38] (Fig. 49.13).

Articular disorders

Osteoarthritis

Osteoarthritis (OA) of the elbow joint is often associated with predisposing factors. There is typically a prior history of trauma, underlying arthropathy,

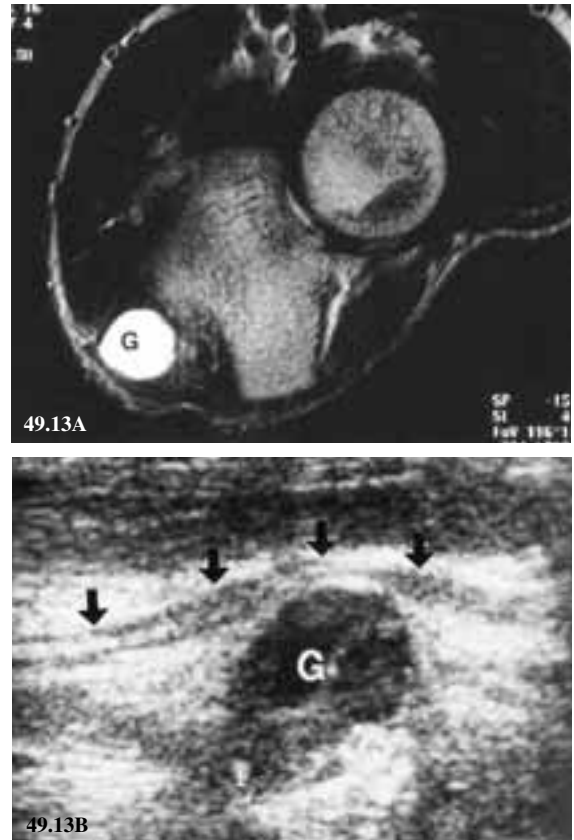


Fig. 49.13: Ganglion within the cubital tunnel. (A) Axial T2-W MR image shows a hyperintense mass (G) containing thin septations. The ulnar nerve is hard to demonstrate. (B) Longitudinal US scan of the cubital tunnel shows the cystic mass (G) (measuring 13.7mm between the electronic calipers) abutting the hypoechoic ulnar nerve (arrows).

or prior septic arthritis. Imaging findings of OA in the elbow are like those of other joints. Sympathetic joint effusion may be seen in inflammatory processes around the elbow, and are possibly due to hyperaemia [33].

Infection

Septic arthritis of the elbow accounts for 3%-13% of all cases of septic arthritis in humans, and is more common in children than in adults. Early diagnosis is very important to prevent rapid destruction of the joint from the action of proteolytic enzymes released from neutrophils, synovial cells, and bacteria [39]. Joint aspiration in a patient with an effusion is mandatory whenever a septic condi-

Sample only

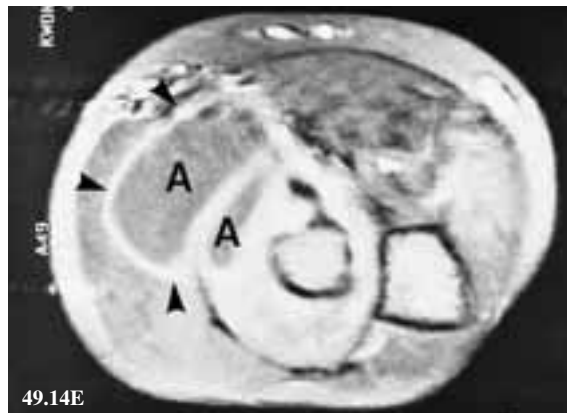
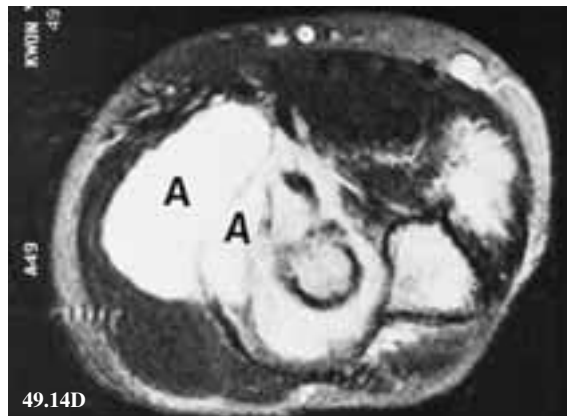
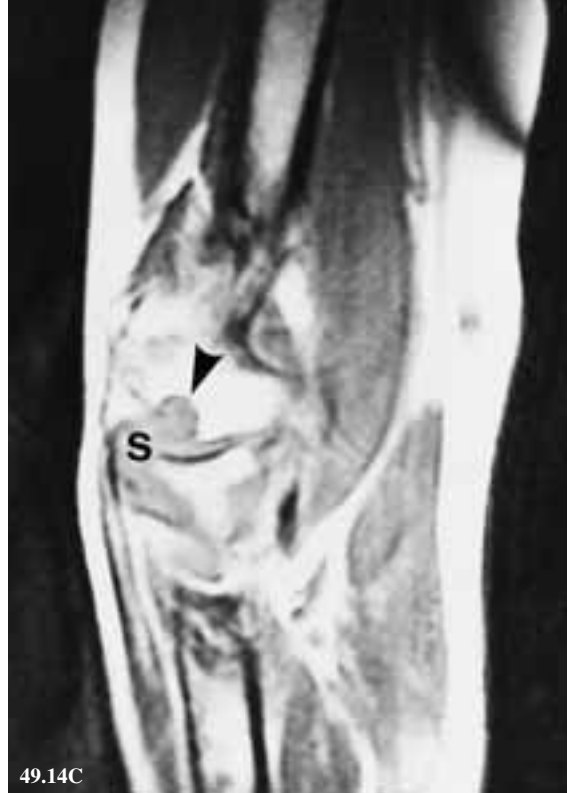
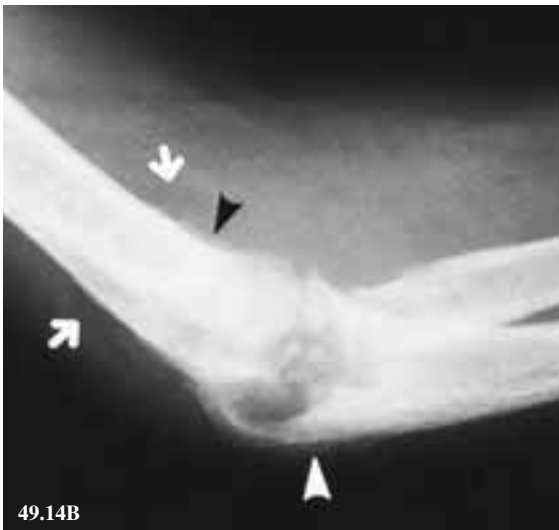


Fig. 49.14: Tuberculous arthritis. (A) AP and (B) lateral radiographs show soft tissue swelling, positive anterior and posterior fat pad signs (arrows), osteoporosis, multiple bone erosions, and periosteal reaction (arrowhead). (B) Sagittal T1-W MR image shows bone erosion (arrowhead) at the capitellum, and synovial proliferation (S) within the joint. (D) Axial T2-W MR image shows two hyperintense masses (A). (E) Enhanced T1-W MR image shows that the walls (arrowheads) of the soft tissue masses are enhanced, representing abscesses (A).

tion is suspected. For this purpose, an ultrasonographic-guided procedure is very useful in the early stage of joint diseases. Ultrasonographical findings of arthritis are an irregular articular surface, elevation of fat pads due to joint distention, fine floating hyperechoic foci in the fluid (probably due to haemorrhage, pus and debris), and synovial proliferation with variable capsule thickness [21,22,40,41]. On MRI imaging, inflamed synovial proliferation is usually hyperintense on T2-weighted images, and shows good enhancement [29]. MR imaging provides a global view for evaluating not only intra-articular and peri-articular pathologies, but also the presence and extent of underlying osteomyelitis. Thin, uniform subchondral oedema and enhancement may be seen, presumably related to hyperaemia, which does not necessarily indicate presence of osteomyelitis [33].

Three-phase bone scintigraphy is very sensitive for the diagnosis of osteomyelitis, but it may be limited in children by uptake of radioisotope at the growth plates. This may be confused with uptake related to infection. MR imaging findings of osteomyelitis are replacement of the normal marrow fat signal on T1-weighted images, hyperintensity of the marrow and soft tissue due to oedema on T2-weighted images, and enhancement of inflamed tissue. Necrosis and abscess in the bone and soft tissue are seen as hyperintense areas on T2-weighted images. The abscess wall is typically rim-enhanced with lack of central enhancement [33]. Tuberculous infection around the elbow commonly involves both bone and adjacent joint, and is hard to differentiate from other chronic infections. Tuberculous infection typically shows bone destruction with cyst-like rarefaction, mild marginal sclerosis, rarely sequestrum, and no periosteal reaction on radiographs (Fig. 49.14).

Loose bodies

The elbow, after the knee, is the most common

joint to have loose bodies. These may result from detachment following osteochondral trauma, osteochondritis dissecans, osteophytes of degenerative joint disease, inflammatory arthritis, synovial osteochondromatosis, and secondary to unknown causes [41]. **Synovial osteochondromatosis** is a self-limiting benign disease with idiopathic cartilaginous metaplasia of subsynovial soft tissue. Radiographs show multiple calcified or ossified nodules within a widened joint space, effusion, bony erosions, and a positive fat pad sign. In one-third of cases of synovial osteochondromatosis, there is no mineralisation of the cartilaginous foci present, making the radiological diagnosis difficult. In such circumstances, differentiation from other joint pathologies is difficult.

On radiographs, osteophytes and periarticular ossification may be confused with intra-articular loose bodies. CT is thus more helpful than radiographs, although non-calcified loose bodies cannot be depicted on either radiographs or CT. On US, loose bodies are demonstrated as focal echogenic structures lying within the joint cavity, completely separated from other joint structures [42,43]. Large osseous fragments may contain fatty marrow [29]. On MR imaging, small loose bodies may be difficult to visualise and differentiate from other foci of signal void, such as synovial fibrosis, air bubbles, and blood vessels within a joint cavity, especially where there is no joint effusion [20,29,44,45]. The air bubble has a characteristic hyperintense margin adjacent to the signal void due to the magnetic susceptibility artifact that is not found in real loose bodies [20].

Osteochondritis dissecans is caused by chronic lateral impaction to the capitellum or radial head, especially in adolescent baseball pitchers with repeated valgus stress to the elbow. Without treatment, this eventually progresses to osteoarthritis [20]. The earliest radiographical finding is a focal radiolucency at the subchondral area of the capitellum.

lum, which later becomes a subchondral bone island demarcated by a rarefied zone [19,20]. It can be divided into two types: unstable or stable. Stable lesions are treated conservatively, whereas unstable lesions and loose bodies are usually treated surgically. An unstable osteochondral fragment is encir-

led by fluid on T2-weighted or STIR images [19,20,29,45,46].

Panner disease or osteochondrosis of the capitellum, commonly occurs secondary to trauma. It represents an avascular necrosis of the capitellar ossification centre. Subsequent follow-up reveals normalisation with little or no residual deformity of the articular surface of the capitellum. MR imaging shows fragmentation and hypointensity of the epiphysis on T1-weighted images, similar in appearance to Legg-Calve-Perthes disease of the hip [19,20,46].

Osteochondritis dissecans should be distinguished from pseudodeflect of the capitellum (a normal variant), and Panner disease [19,20,46,47]. Osteochondritis dissecans is typically seen in the 13-16 year age range, whereas Panner disease is typically seen in the 5-11 year age range, before ossification of the capitellum is complete [20]. Loose bodies are formed in osteochondritis dissecans but are usually not seen in Panner disease. The articular surface in Panner disease remains intact, and does not undergo fragmentation or loose body formation. Osteochondritis dissecans typically involves the anterior aspect of the capitellum, whereas pseudodeflect of the capitellum is located at the abrupt transition site between the posterolateral margin of the capitellum and the non-articular portion of the lateral humeral condyle.

Tumours

In the elbow, musculoskeletal tumours are relatively uncommon [48,49]. Soft tissue masses in the elbow follow the general caveats for imaging of masses elsewhere in the body [29]. US is limited in its ability to provide a histological diagnosis of a tumour except for cyst, lipoma, neurilemmoma, and haemangioma [29,50-52] (Fig. 49.15). Even when CT and MR imaging are performed, the vast majority of soft tissue tumours remain non-specific, with a correct histological diagnosis reached on the basis

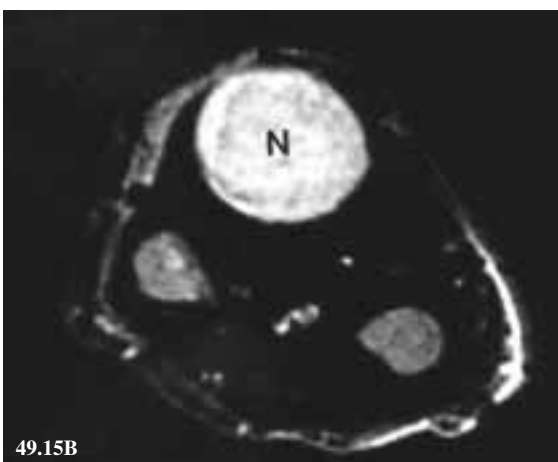


Fig. 49.15: Neurilemmoma. (A) Sagittal T1-W MR image shows a mass (N) of isointense signal intensity. The mass appears to be connected to the ulnar nerve (arrowheads). (B) Enhanced axial fat-suppressed T1-W MR image shows the mass (N) to be heterogeneously enhanced.

of imaging studies in only approximately 25% of cases [48,49]. In these situations, US is very useful for guiding a percutaneous fine needle aspiration and/or biopsy and to avoid blood vessels, nerves, and areas of tumour necrosis. Before performing a percutaneous biopsy, it is obligatory to discuss the biopsy approach with the surgeon who will perform the tumour excision.

HAND AND WRIST

For evaluating pain about the hand and wrist, routine radiographs are the first basic examination usually performed after a careful clinical history and physical examination, although they are non-specific [53-55]. In addition, there are many imaging techniques available to evaluate the underlying causes of wrist pain, including CT, US, MR, arthrography, and scintigraphical scans [56-59]. Different and specific imaging approaches to evaluate each disease presenting with wrist or hand pain is advocated [55].

TABLE 49.1
ABCD'S for Radiographical Analysis
of Joint Diseases

A	Alignment of the bone and joint
B	Bone mineralisation as well as the character of erosions and bony spurring
C	Cartilaginous abnormalities including joint space narrowing
D	Distribution of disease
S	Soft tissue abnormalities such as capsular swelling, synovial proliferation and soft tissue atrophy

[Modified from: Forrester DM, Brown JC. Radiology of Joint Disease. 3rd ed. Philadelphia: WB Saunders, 1987]

Articular and bone disorders

Specific types of joint disease can be diagnosed by examining radiographs, bearing in mind the well-known mnemonic, **ABCD'S** for radiographical joint analysis [53] (Table 49.1). Dedicated radiographs of the feet, spine and sacroiliac joints may be helpful for diagnosing rheumatoid arthritis and its variants [54].

Osteoarthritis

Osteoarthritis (OA) is caused by a softening, fissuring, and fragmentation of the articular cartilage. This results in degeneration and narrowing of the joint space [53,60-62]. Some clinicians prefer to use the term “degenerative joint disease” [54]. In the hands, the distal interphalangeal joint is most commonly involved, followed by the proximal interphalangeal and first carpometacarpal joints [60]. Radiographical findings are joint space narrowing, osteophytes with Heberden nodes, sclerosis of bony margins, and subchondral cyst formation, regardless of whether the cause is primary or secondary [54,61,62]. Secondary osteoarthritis is most frequently caused by previous traumatic injuries. Subchondral cysts may occur and be filled with synovial or mucous fluid, or fibrovascular tissue [54,61]. Cartilage metaplasia may occur at the bony attachments of capsule, ligament, and tendon [54].

Rheumatoid arthritis

Rheumatoid arthritis is one of the most common joint diseases encountered in the hand and wrist. Histopathologically, rheumatoid arthritis is an acute or chronic synovitis, often with marked synovial proliferation, and involves any synovium-lined space, i.e. the joint, tendon sheath, and bursa [53,54,62-64]. Radiographically, it is characterised early in the disease course by fusiform soft tissue swelling and juxta-articular osteoporosis. There is a typical bilateral and symmetrical distribution in some distinct areas, e.g. around the proximal interpha-



Fig. 49.16: Rheumatoid arthritis. AP radiograph of early stage rheumatoid arthritis shows fusiform soft tissue swelling (arrowheads) with typical bilateral and symmetrical distribution. (B) AP radiograph of another patient with advanced rheumatoid arthritis shows diffuse osteoporosis, a soft tissue nodule and a marginal bony erosion at the proximal interphalangeal joint (arrowhead). Joint space narrowing and articular destruction are prominent in the wrist, intercarpal, and carpometacarpal joints.

langeal, metacarpophalangeal, radiocarpal, and intercarpal joints [64] (Fig. 49.16A). Small marginal erosions of bone initially occur near the capsular attachment at the bare area of the joints, i.e. points of absence of overlying cartilage [54]. Pressure erosion of the ulnar styloid process is a typical finding. Later, joint space narrowing, articular destruction, and ligamentous laxity due to on-going inflammation may result in ulnar-deviated

malalignment of the bone and joints, and eventual ankylosis [54,63] (Fig. 49.16B).

Bone erosions and synovitis are definitely visualised earlier with MR imaging and US than with radiographs [62,64-67]. On T2-weighted MR imaging, synovitis in rheumatoid arthritis is manifested as accumulation of hyperintense fluid, conforming to the known contour of the synovial space [62]. Pannus is seen as thickening of the synovium, with hyperintensity lower than that of fluid on T2-weighted images. It may be difficult or impossible to differentiate synovial proliferation from effusion without performing contrast studies or special MR sequences [62]. After intravenous administration of Gd-DTPA, enhancement of the hypervascular pannus can be differentiated from synovial fluid. Chronic synovitis may be depicted as having intermediate signal intensity on both T1- and T2-weighted images, as the inflamed tissue is less prominent and may contain more fibrosis. Superficial erosions of the cortices of bones may be seen as hyperintense defects with a scalloped appearance [62].

Septic arthritis

Septic arthritis is typically monoarticular, especially at the metacarpophalangeal joints in hands. It



Fig. 49.17: Avascular necrosis of the scaphoid. (A) AP radiograph shows that the proximal portion (P) of the scaphoid bone is relatively sclerotic. Fracture line (arrowheads) is clearly visualised. (B) Coronal T1-W MR image shows loss of normal fatty marrow signal in the fractured proximal fragment (P). (C) Coronal T2-W MR image shows inhomogeneous-hyperintensity (arrowheads) of the fractured proximal fragment of the scaphoid, suggestive of necrosis, oedema or granulation tissue. Joint effusion is present.

often results from direct implantation of bacteria by human bites [53,54]. Untreated septic arthritis causes rapid destruction of the joint cartilage. Widening of the joint space may be seen in the acute stage as the inflamed cartilage becomes oedematous. Subsequent synovial hypertrophy and bone erosions may mimic those seen in rheumatoid or tuberculous arthritis.

Low-virulent bacterial infection such as tuberculous or fungal infection leads to relative cartilage preservation with earlier demineralisation and erosion of the bones. Recent advances in the development of surface coil and imaging techniques in MR imaging provide anatomical details of the bone, joint abnormalities, and soft tissue abnormalities [59,66]. For the early detection of osteomyelitis,

MR imaging is as sensitive as bone scintigraphy. The latter technique has long been recognised as being superior to radiographs.

Osteonecrosis

Osteonecrosis, commonly involving the lunate, proximal segment of the scaphoid, and other carpal bones, is accurately depicted in early clinical course using MR imaging [59]. The necrotic portion of the bone is manifested as a loss of normal fatty marrow signal intensity on T1-weighted images, and low or inhomogeneously-high signal intensity on T2-weighted images (Fig. 49.17). Inhomogeneously-high signal on T2-weighted images may be interpreted as a mixture of necrosis and oedema, or granulation tissue at the junction between the

necrotic and revascularised bone [58]. The areas with enhancement may represent retained or revascularised portions, which can be regarded as being indicative of a good prognosis [59,68]. Collapse of the articular surface of the involved bone and displacement of the resulting fragments in the later stage is best observed on MR imaging.

Tear

Tear of the triangular fibrocartilage complex (TFC) is seen on MR imaging as interruption of the normal hypointense signal of the TFC by a zone of intermediate or hyperintense signal with irregular, frayed margins [59,69,70]. The adjacent extensor carpi ulnaris appears irregular in contour with a fusiform swelling and non-homogeneous signal, when a partial tear or tendinitis is present (69-71). Not only does MR imaging show TFC perforation better than does arthrography, but it also allows evaluation of other wrist disorders of potential interest to the surgeon [71,72].

Ligament and tendon lesions

Wrist and carpal instabilities result from abnormalities of bones and ligaments that may be due to many causes [73,74]. The lunate is the key landmark in the diagnosis of carpal instabilities. It is importantly to note that not all carpal malalignments on radiographs represent carpal instability, even

though dynamic and stress views are obtained [73,74]. High-resolution MR imaging using various techniques is evolving as a useful tool for assessing the anatomical and functional integrity of the ligaments, although it has some limitations [59,75,76].

Gamekeeper's thumb is a tear of the ulnar collateral ligament of the thumb induced by repetitive microtrauma, or by violent hyperabduction injuries at the metacarpophalangeal joint, most commonly caused by skiing [77]. After rupture, the torn ligament may remain beneath the adductor aponeurosis in cases of partial tear, and can usually be treated conservatively. However, the torn edge of the ligament may be trapped superficially over the adductor aponeurosis, making normal healing impossible [77-80]. It is therefore very important to differentiate a displaced tear (Stener lesion) from a non-displaced tear because surgical intervention is mostly required for the treatment of Stener lesion. Both MR imaging and US are valuable methods for this purpose [57,58,77-80].

The distinction between tendinitis and tenosynovitis is important because of the differences in their treatment. Tendinitis is usually treated with rest and non-steroidal anti-inflammatory medications, whereas tenosynovitis may require steroid injection or surgery [57]. US is the favoured imaging modality for evaluating tendon lesions and assessing the relationship of the tendon with adjacent neurovascu-

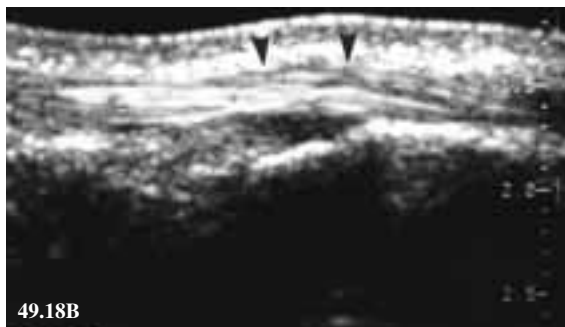


Fig. 49.18: De Quervain disease. (A) Longitudinal US scan of the 1st extensor compartment of the wrist shows hypoechoic nodular enlargement (arrowheads) of the extensor pollicis brevis and abductor pollicis longus tendons. Dynamic US examination showed limited motion of the tendon. (B) Repeat longitudinal US scan shows that the tendons are normalised in echo-pattern and contour (arrowheads) two years later.

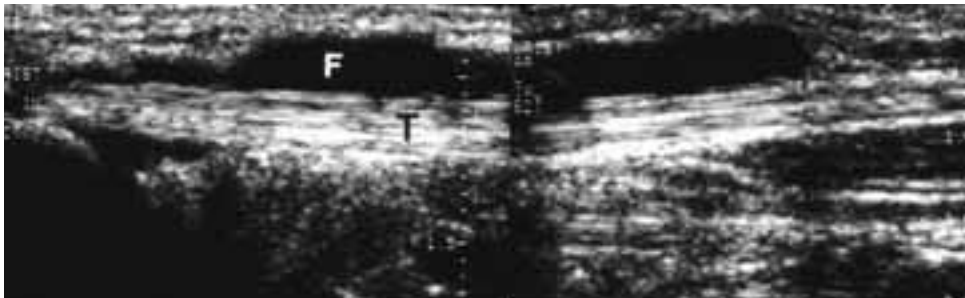


Fig. 49.19: Tenosynovitis of the flexor carpi radialis tendon. The flexor carpi radialis tendon (T) at the distal forearm shows surface irregularity within a fluid-filled tendon sheath (F).



Fig. 49.20: Giant cell tumour of the tendon sheath. (A) Anteroposterior and (B) lateral radiographs show a well-defined bone erosion (arrow) located along the ventral aspect of the head of the proximal phalanx of the middle finger. (C) Sagittal T2-W MR image shows the hyperintense mass between the eroded bone (arrow) and the flexor tendon (arrowheads).

lar structures. MR imaging also plays a role in evaluating a tendon abnormality either in isolation or in association with other lesions of the bone and joint. Tendon rupture appears on US and MR imaging as either a complete or partial discontinuity of the tendon, focal defect within the tendon substance with accompanying inflammation, and fluid collection or haemorrhage at the tear site [57,58,81-83].

Stenosing tendinitis, including de Quervain disease, shows increased tendon thickness or synovial thickness, or both. Tendon echogenicity may also change (Fig. 49.18). More information about the lesions can be obtained when local pressure is applied with the transducer, and ultrasonographical physical examination is performed during a passive or active motion of the tendons in flexion and extension [81,84,85]. MR imaging and US findings of tenosynovitis are thickening of the tendon sheath, synovial proliferation within the sheath, peritendi-

nous fluid collection, and associated contour change of the tendon (thickening or thinning) [57,58,81,84-86] (Fig. 49.19). On transverse sections, the tendon is surrounded by fluid, resulting in a target appearance [86].

Giant cell tumour of the tendon sheath, a localised form of pigmented villonodular synovitis, is usually hypo- or isointense on T1-weighted MR images and moderately hyperintense on T2-weighted MR images. Occasionally, pressure from the lesion may cause local bony erosions that may be seen on radiographs [57,58,83,87]. Pigmented villonodular synovitis may sometimes present as a hypointense mass on both T1- and T2-weighted images, according to the T1 and T2 values of the tissues related to the haemosiderin-derived pigment deposited in the tumours [87] (Fig. 49.20).

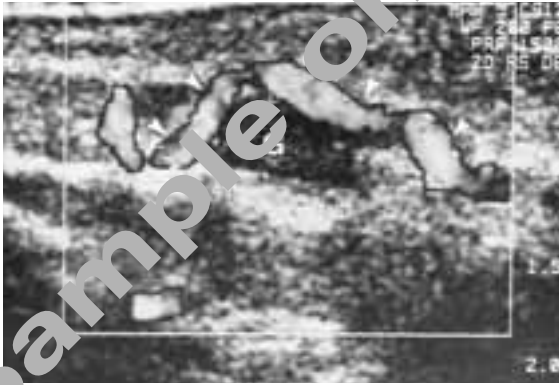


Fig. 49.21: Ganglion. Longitudinal US scan shows an anechoic mass (G) around the flexor tendon of the ring finger. Adjacent vessel (arrowheads) is displaced by the ganglion.

Carpal tunnel syndrome

Carpal tunnel syndrome is most often related to degenerative diseases of the fibrous structures. It is caused by overuse related with job or sporting activities, direct trauma, tenosynovitis, space-occupying lesions, and medical diseases such as diabetes mellitus and inflammatory arthritis. This is mostly a clinical diagnosis confirmed by electromyography (EMG) of the median nerve, and is easily corrected by simple surgical procedures [88]. MR imaging is reserved for patients with discrepancy between clinical and EMG findings, or recurrent symptoms following surgery [89].

MR imaging with proton density or T2-weighted sequences may show that the nerve is diffusely hyperintense. There may be swelling of the nerve proximal to the level of compression, flattening of the nerve at the compression site at the level of the hamate, and palmar bowing of the flexor retinaculum. Ultrasonographically, the nerve appears deformed, with loss of the hyperechoic fascicular echo-texture. It is important to be aware that the size of the median nerve at a single level is not diagnostically useful because of individual differences in size of the nerve [57,58,88].

Tumours and tumour-like lesions

Most of the bone tumours in the hand and wrist

are benign. These include chondroma, osteoid osteoma, osteochondroma, giant cell tumour, in order of frequency of incidence. Rarely, metastatic foci from malignancies in remote sites are found in the bones of the hand and wrist [90]. Radiographs are essential to evaluate bone tumours, and underlying or co-existing soft tissue abnormalities. They also help to reveal the presence and nature of soft tissue calcifications that may be suggestive, and are at times very characteristic, of a specific diagnosis.

Most of the soft tissue tumours in the hand and wrist are small and benign, thus US provides information about their origin, nature, size, and the relationship with other adjacent anatomical structures [57,58,91] (Fig. 49.21). A specific diagnosis can be obtained, or strongly suspected, from the characteristic MR features found in certain conditions such as ganglion, haemangioma, arteriovenous malformation, giant cell tumour of the tendon sheath, and lipoma [90,92]. MR imaging provides essential information for pre-surgical planning, including: the depth of extension of the mass, tumour size, and relationship to adjacent neurovascular structures. The histology of the masses cannot however always be predicted [59,87,90].

Foreign bodies in the hand may be diagnosed with high index of suspicion and a proper history. Multiple radiographical views are always necessary to detect and distinguish foreign bodies from other soft tissues and bony structures. If the radiographs are normal, US is very useful in the detection of non-radio-opaque foreign bodies, such as wood or glass fragments [57,58]. Foreign bodies appear as hyperechoic foci with acoustic shadowing, although the size of the object and the experience of the operator are keys to recognising and distinguishing a foreign object from normal structures. The foreign body usually has surrounding inflammatory changes and fluid collections. By turning and adjusting the transducer back and forth over the object, even a small 3 mm to 4 mm size foreign body is readily seen on

US. The information obtained from US provides an intraoperative guidance for surgical removal.

Glomus tumours arise from the neuromyoarterial glomus located in the subungual aspect of the finger [58]. US shows a solid homogeneously-hypoechoic mass with hypervascularity beneath the nail [53,94] (Fig. 49.22). Most glomus tumours are iso- or slightly hyperintense to the dermal layers of the nail bed on T1-weighted images and strongly hyperintense on T2-weighted images. The signal intensity of the tumour is usually homogeneously enhanced [94].

HIP

The hip is an extremely stable ball-and-socket joint with a primary role in weight-bearing and gait. The globular femoral head articulates with the cup-shaped fossa of the acetabulum. The acetabular cavity is hemispherical in shape and has an elevated bony rim. A fibrocartilagenous labrum is attached to the bony rim, resulting in deepening of the acetabular cavity. The articular capsule is strong, and encircles the joint and much of the femoral neck. Ligaments are seen as thickening of the capsule. They include the iliofemoral, pubofemoral, and ischiofemoral ligaments, and add strength to the articular capsule. Accurate assessment of disorders of the hip depends on

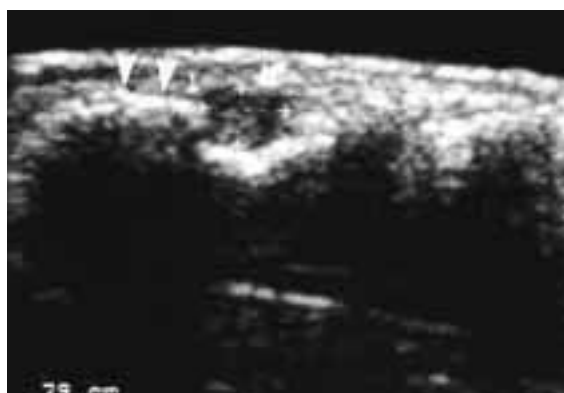


Fig. 49.22: Glomus tumour. Longitudinal US scan taken at the radial aspect of the ring finger tip shows a tiny hypoechoic nodule (curved arrow and between electronic calipers) at the root of the nail (arrowheads).

imaging techniques. A variety of imaging methods, including radiography, arthrography, US, bone scintigraphy, CT and MR imaging, can be used in the evaluation of disorders of the hip [95].

Avascular necrosis

Avascular necrosis (AVN) or osteonecrosis of the femoral head is a common disease with significant clinical consequences [96]. The causative factors leading to AVN of bone include trauma, corticosteroid medication, alcoholism, connective tissue diseases, and haematological and metabolic disorders [95]. Regardless of the cause, the final pathway in the genesis of AVN is the same, namely: compromised blood supply to the femoral head, leading to the death of haematopoietic, osteocytic, and adipose tissue elements. Conventional radiographs had been the standard method for the detection and staging of AVN, although radiographs are insensitive for both small lesions and early AVN [97]. After the development of a sclerotic rim of reactive bone at the ischaemic-viable bone junction, radiographs show positive findings. Conventional tomography and CT scanning are also not reliable in the diagnosis of early AVN of the femoral head. Bone scintigraphy is a sensitive method for the detection of AVN when optimally performed, but the scintigraphical findings lack specificity. Pinhole collimation or single photon emission computed tomography improves the sensitivity. MR imaging is highly sensitive to changes in the composition of bone marrow, and appears best suited to the detection of the early stages of AVN [95].

MR imaging finding of a circumscribed signal abnormality with a hypointense rim in the subchondral location is virtually diagnostic of AVN. The area of ischaemic marrow may be surrounded by a reactive interface that is characterised

by hypointense signal on T1-weighted MR images (Fig. 49.23). The “double line” sign consists of a hypointense outer rim and a hyperintense inner rim on T2-weighted MR images, and is also considered specific for AVN [98]. MR imaging abnormalities are somewhat variable in their time of occurrence. The central region within the infarcted area may initially reveal signal characteristics of normal fat, but with chronicity, its signal characteristics may change, resembling those of fluid, haemorrhage, or fibrosis. They depend on alterations of the fat cells in the bone marrow. Fat cells are more resistant to ischaemia, surviving for 2 days to 5 days after the insult [95]. The MR imaging characteristics of AVN of the femoral head may be variable. A diffuse pattern of bone marrow oedema, identical to that of transient bone marrow oedema, may be identified in the early stages of the process. Subsequently, a more focal process within the femoral head allows a more specific diagnosis [99].

Transient bone marrow oedema

Transient bone marrow oedema of the hip is a painful, self-limited, idiopathic process that has proved to be more common in men than in women. It affects either the right side or the left side, and occasionally, migrates from one side to the other.

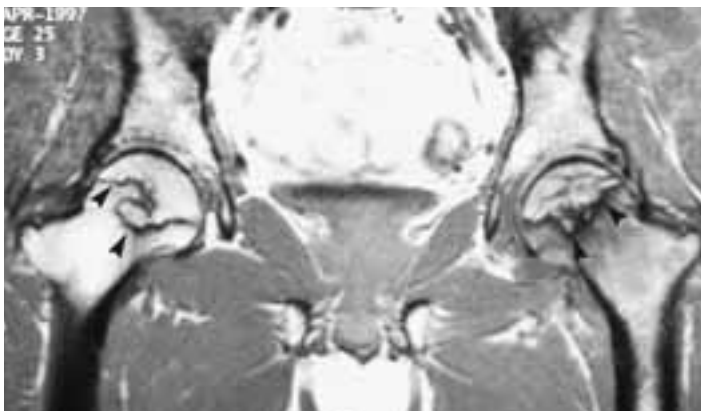


Fig. 49.23: Avascular necrosis of the femoral head. Coronal T1-W MR image shows typical changes of avascular necrosis in the both femoral heads. Serpentine regions of hypointensity (arrowheads) surround a central isointense region. Marrow oedema seen as hypointense areas is evident in the left femoral neck.

Transient pain and limitation of motion of the hip are associated with radiographically-evident osteopenia, and an MR imaging pattern consistent with bone marrow oedema [95]. The relationship between transient bone marrow oedema and AVN of the femoral head is controversial. It is important to recognise the difference between bone marrow oedema without AVN, and that with AVN [100]. The former is a hypervascular, usually self-limiting disorder, whereas the latter is unequivocally ischaemic.

The differential diagnosis includes AVN, septic arthritis, inflammatory arthritis, synovial osteochondromatosis and pigmented villonodular synovitis. Although AVN may be present when radiographical findings are normal, MR imaging demonstrates signal abnormality in the femoral head that progresses into a well-defined hypointense geographical area. Septic arthritis eventually shows joint space narrowing and osseous erosion. Inflammatory arthritides such as rheumatoid arthritis causes an intense synovial inflammation, resulting in osseous and cartilaginous erosions. Symmetrical involvement is also more characteristic of rheumatoid arthritis [101].

Legg-Calvé-Perthes disease

The aetiology, radiographical classification, and treatment of Legg-Calvé-Perthes (LCP) disease remain controversial. LCP disease may be radiographically silent for the first 3 months to 6 months. MR imaging is useful for the assessment of a variety of causes of hip pain in the child, including LCP disease. MR imaging reveals a number of findings, including thickening of cartilage of the acetabulum and femoral head, physeal irregularity, transphyseal bone bridging, loss of containment of the femoral head within the acetabulum, changes of signal intensity in the marrow and epiphyseal cartilage, synovial inflam-

mation, and secondary osteoarthritis [95].

Occult fractures

Some acute fractures, trabecular microfractures, and stress fractures are difficult to diagnose, not only clinically but also radiographically. The application of other imaging methods, such as bone scintigraphy and MR imaging, for the detection of these fractures has received a great deal of attention [95]. Bone scintigraphy has proved to be more sensitive than radiography in confirming a femoral neck fracture. MR imaging appears to be equally sensitive and far more specific for the detection of fractures of the femoral neck [102]. A negative MR imaging examination effectively eliminates the diagnosis of such fractures. The MR imaging characteristics of an undisplaced fracture of the femoral neck are a well-defined linear hypointense zone on T1-weighted MR sequences (Fig. 49.24). It may be surrounded by a broader and poorly-defined hypointense zone, consistent with marrow oedema [103]. On T2-weighted MR images, the fracture line may remain hypointense, but the oedematous zone is hyperintense [95].

Developmental dysplasia of the hip

Developmental dysplasia of the hip (DDH) is defined as deformity of the acetabulum of varying degrees. The femoral head often migrates laterally and superiorly. Diagnosis in the first few months of life allows conservative treatment, with complete resolution expected in most cases [104]. Selection of appropriate imaging techniques in patients with DDH depends on age, and differs for diagnostic versus management situations. Conventional radiographs prior to 6 weeks of age have a high false negative rate because most of the hip consists of non-ossified radiolucent cartilage. The value of US in diagnosis and follow-up of DDH is well established, and this method should currently be considered the imaging method of choice for objectively



Fig. 49.24: Occult fracture. (A) AP radiograph shows subtle sclerosis (arrow) at the femoral neck. (B) Coronal T1-W MR image shows the fracture line (arrow).

documenting the condition and monitoring the effectiveness of treatment. The advantages of US include detailed depiction of the cartilaginous femoral head and its relationship to the bony and cartilaginous acetabulum, and provides dynamic information documenting subluxation, dislocation, and reduction [105].

MR imaging can accurately depict the most important determinants of stability in the neonatal hip [106, 107]. These include femoral head shape, acetabular shape, position of the labrum, invagination of the joint capsule by the iliopsoas tendon, degree of femoral and acetabular anteversion, and the position of the transverse ligament. Coronal images are optimal for depicting the clinically-important structures of the acetabular roof, including the labrum. Axial images are suited for demonstrating the anterior and posterior structures of the joint. MR imaging should not be used for initial diagnosis or evaluation of routine DDH but should be reserved for complicated cases in which initial treatment was unsuccessful [106].

Labral abnormalities

Acetabular labral lesions are a considerable cause of hip pain in adults with DDH or with a history of hip trauma [108-110]. A spectrum of acetabular labrum and adjacent bone abnormalities appear to relate to either acute injury or chronic stress. The labral abnormalities may take the form of acute tears, chronic deformation, cyst formation, or degeneration. The osseous abnormalities include cyst formation or fragmentation [95]. The role of MR imaging in the assessment of the torn acetabular labrum is not clear at the present time. Use of an intra-articular contrast agent is necessary to differentiate torn and detached labra from other forms of labral lesions [108,111,112]. This includes separating internal signal intensity abnormalities secondary to tears from those due to other causes, as well as separating the normal signal intensity at the labral-acetabular junction from that secondary to detachment [113].

The sensitivity and accuracy of MR arthrography for detection of labral tears and detachments is 90% and 91%, respectively, versus 30% and 36%



Fig. 49.25: Synovial osteochondromatosis. (A) AP radiograph shows multiple calcified bodies (arrows) around the femoral neck. (B) Coronal T2-W MR image shows joint distention with multiple intra-articular bodies (arrow).

for non-arthrographical MR images [108]. The significance of morphologic changes in the labrum is uncertain. MR images reveal perilabral cysts which appear as well-defined hypointense masses on T1-weighted MR images, and have hyperintense signal on T2-weighted MR images. These cysts may accompany a pathological labral condition, especially detachment [114]. Identification of a cyst around the hip joint should raise the possibility of an underlying acetabular labral tear [114-116]. These cysts are typically extra-articular in location, and may erode into the adjacent bone. They may or may not fill with the injected contrast agent at the time of MR arthrography [113]. Intra-labral degenerations may be associated with regions of hyperintensity on MR images. The occurrence of labral alterations in asymptomatic persons, as has been verified in the glenohumeral joint, may ultimately limit the clinical usefulness of the MR examination.

Arthropathies

The hip joints are a target for many arthritides. Primary and secondary osteoarthritis are common. The inflammatory arthritides, especially rheumatoid arthritis, infective arthritis and calcium pyrophosphate dihydrate deposition (CPPD) disease, involve the hip joint as well. Pigmented villonodular synovitis and synovial chondromatosis (Figure 49.25) also occur in the hip [95]. Imaging studies provide useful information for the diagnosis, assessment of the lesion extent, pre-operative planning and follow-up. Conventional radiography is the primary imaging modality for suspected arthropathies of the hip. Osteoarthritis is readily identified by joint space narrowing, osteophytosis, sclerosis, and subchondral cyst formation. Inflammatory arthritis shows concentric joint space narrowing, producing an axial migration pattern, as well as articular erosions. MR imaging and CT may be valuable in assessing arthropathies [96].

Calcific tendinitis

Calcium hydroxyapatite crystal deposition may involve the tendons and bursae of the hip. Calcific deposits are frequent at the sites of the gluteal insertions into the greater trochanter, and in the surrounding bursae. Calcific deposits may relate to tendinous structures, such as the rectus femoris (Fig. 49.26), vastus lateralis, piriformis, adductor



Fig. 49.26: Calcific tendinitis. (A) AP radiograph shows a round calcification (arrows) adjacent to the acetabulum. (B) Coronal PD-W MR image shows the site of calcification as a hypointense area (arrow), located in the tendon of the rectus femoris muscle (open arrow).



Fig. 49.27: Trochanteric bursitis. (A) Coronal T2-W and (B) enhanced axial T1-W MR images show the distended trochanteric bursa (arrows) which contains rice bodies (arrowheads).

magnus and biceps femoris tendons [95].

Bursitis

Inflammation of the iliopsoas bursa, ischial bursa and trochanteric bursa are not infrequently encountered. Iliopsoas bursitis is usually associated with an abnormality in the adjacent hip. Ischial and trochanteric bursitis may be related to strenuous activity and irritation. Infectious involvement, such as that due to tuberculosis, may also be encountered. US and MR imaging are the optimal imaging techniques for assessment of these bursal abnormalities [95] (Fig. 49.27).

Bone tumours and tumour-like lesions

A variety of bone tumours and tumour-like lesions are encountered around the hip. Simple bone cyst (Fig. 49.28), osteoid osteoma, aneurysmal bone cyst, osteochondroma, chondroblastoma and lipoma are relatively-common benign lesions of the hip. Of the malignant bone tumours, metastasis, osteosarcoma, chondrosarcoma and lymphoma are frequently seen. As in

other areas of the musculoskeletal system, the most important imaging study is conventional radiography. CT is useful in assessing bony characteristics of a lesion, if the anatomy is complex or partly obscured. The intraosseous and extraosseous extent of a primary bone lesion can be effectively evaluated by both CT and MR imaging [96].

KNEE

In the knee joint, three functional spaces exist, namely: the medial tibiofemoral space, the lateral tibiofemoral space, and the patellofemoral space. The vulnerability of the knee, the largest joint in the body, makes it liable to develop many kinds of diseases throughout life. The major disease processes that affect the knee joints are discussed.

Arthritides

The clinical manifestations and laboratory data, in conjunction with the radiographical findings, are of significant help in making the diagnosis of a specific arthritic process [117].

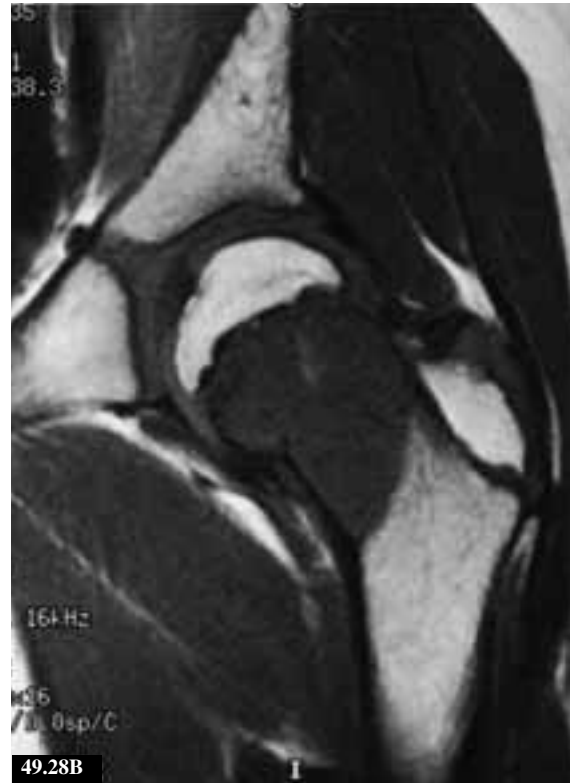


Fig. 49.28: Simple bone cyst. (A) AP radiograph shows a large osteolytic lesion (arrows) at the femoral neck. (B) Coronal T1-W, (C) fat-suppressed T2-W and (D) enhanced fat-suppressed T1-W MR images show a fluid-filled cystic lesion with internal septations.



Fig. 49.29: Osteoarthritis of the knee. (A) Anteroposterior and (B) lateral radiographs of the knee show asymmetrical narrowing of the medial joint space, subchondral sclerosis and marginal osteophytes. An irregularly-marginated calcified opacity is noted in the suprapatellar bursa.

Osteoarthritis

The knee is a complex joint comprising three major compartments, each of which may be affected by degenerative changes. The radiographical features are narrowing of the joint space, subchondral sclerosis, osteophytosis, and subchondral cyst formation. The standard anteroposterior and lateral projections of the knee are sufficient to demonstrate these processes (Fig. 49.29).

Rheumatoid arthritis

Any of the large weight bearing and non-weight bearing joints may be affected by rheumatoid arthritis. Certain radiographical features that are characteristic of this inflammatory process can be identified. In the early stage of the disease, osteoporosis is localised to periarticular areas. With progression

of the condition, a generalised osteoporosis is observed. Joint space narrowing is usually a symmetrical process with concentric joint space narrowing. Marginal erosions, without evidence of subchondral sclerosis or osteophytosis, may be present. Synovial cysts are seen as radiolucent defects, usually in close proximity to the joint. Joint effusion is a feature.

Pigmented villonodular synovitis

Pigmented villonodular synovitis is a monoarticular synovial disease that affects either the joint or tendon sheath in young adults. The knee is involved in 80% of cases with articular disease. Articular disease may be divided into two forms, namely: diffuse and nodular. Typical radiographical findings in pigmented villonodular synovitis include a non-calcified synovial soft tissue mass, subchon-

dral and juxta-articular erosion, and cysts, normal bone density, normal joint space, and lack of hypertrophic bone formation [118]. Because of the presence of haemosiderin pigmented villonodular synovitis are typically hypointense on both T1- and T2-weighted images.

Lipoma arborescens

Lipoma arborescens is a rare intra-articular lesion characterised by villous lipomatous proliferation of the synovium, usually involving the suprapatellar pouch of the knee joint. MR images show villous lipomatous proliferation with signal intensities similar to those of fat on T1- and T2-weighted images, mass-like subsynovial fat deposition, joint effusion, erosive bone changes at the articular margins, associated synovial cysts, and degenerative changes [119].

Meniscal tears

Meniscal tears are generally divided into two major types. The first is the acute traumatic tear which predominantly occurs in young athletes, and is thought to be secondary to crush and twisting injuries of the menisci. The second occurs in older individuals, and is secondary to degenerative disease [120]. Meniscal tears may also be divided, based on the morphology of the tear. This includes longitudinal tears, transverse tears, and oblique tears (Fig. 49.30), according to surface tear pattern. A bucket handle tear is a vertical longitudinal tear in which the inner fragment is displaced towards the intercondylar notch of the knee. A discoid lateral meniscus is said to be present if three or more 5 mm thick contiguous sagittal images reveal continuity of the anterior and posterior horns of the lateral meniscus. Peripheral tears and peripheral



Fig. 49.30: Oblique tear of the lateral meniscus with a meniscal cyst. (A) Coronal PD-W MR image shows a band-like area of hyperintensity in the lateral meniscus, and a cystic lesion at the lateral margin of the meniscus. (B) Sagittal PD-W MR image shows a band-like hyperintense area in the lateral meniscus representing the meniscal tear.

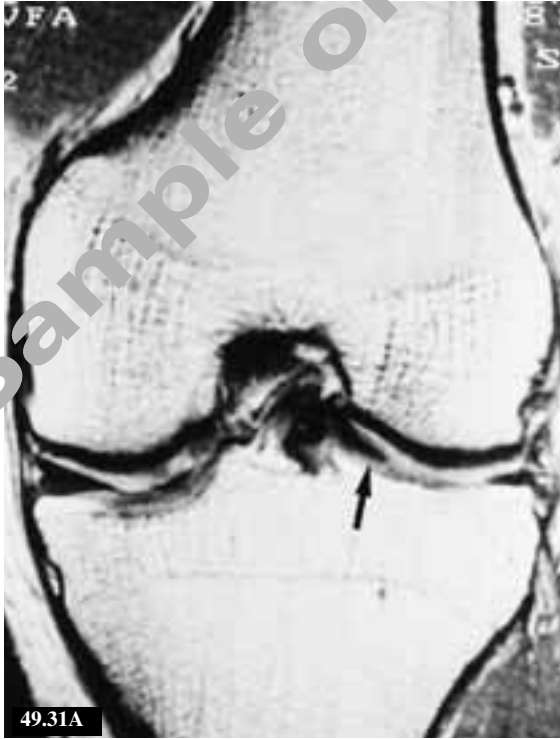


Fig. 49.31: Meniscal tear of discoid lateral meniscus. (A) Coronal PD-W MR image shows displacement of the torn segment (arrow) of the lateral meniscus. (B) Sagittal PD-W MR image shows the torn segment (arrow) at the intercondylar region.

oblique tears are the most common types of discoid lateral meniscal tears, and displacement of the torn meniscal segment is frequent [121] (Fig. 49.31). Meniscal cysts result from extrusion of joint fluid through an oblique meniscal tear into the surrounding tissues. MR imaging of meniscal cysts shows a fluid collection contacting the periphery of the meniscus, adjacent to an oblique meniscal tear [122].

Ligamental tears

Anterior cruciate ligament

Anatomically, the anterior cruciate ligament fibres are divided into two bands. The anteromedial band inserts at the anteromedial aspect of the tibial attachment, and the posterolateral band inserts at the posterolateral aspect. Disruption of the anterior cruciate ligament most often occurs in its mid-portion, although occasionally, the ligament is avulsed from its femoral insertion. In the presence of a partial- or full-thickness tear, irregularity or a wavy contour of the anterior margin of the anterior cruciate ligament is often demonstrated on sagittal images. In addition, increased signal within the substance of the ligament, presumably representing blood or oedema, is present. With a complete tear, discontinuity of the fibres is seen, as well as abnormal orientation of the torn ends [123] (Fig. 49.32).

Posterior cruciate ligament

Considerably more force is required to produce a tear of the posterior cruciate ligament than the anterior cruciate ligament. The most common site for a tear is the mid-portion of the ligament. Complete tears are seen as fraying at the site of the tear on the sagittal image, whereas incomplete tears are noted as areas of increased signal within the ligament.

Medial collateral ligament

The structures comprising the medial collateral



Fig. 49.32: Complete tear of the anterior cruciate ligament. (A) Sagittal PD-W MR images show (A) complete discontinuity of the proximal portion of the anterior cruciate ligament (curved arrow) and (B) mild buckling of the posterior cruciate ligament (arrowhead).

ligament complex are most readily assessed in the coronal plane. Its attachment to the medial femoral epicondyle is usually more easily identified than its insertion on the tibia. In severe injuries, the medial collateral ligament is thickened and is often serpiginous. The normally hypointense signal of the medial collateral ligament is lost (Fig. 49.33).

Lateral collateral ligament

Complete tears of the lateral collateral ligament occur either in mid-substance or as an avulsion from the fibular head. Significant effusion indicates the presence of an associated capsular or cruciate ligament injury, since the lateral collateral ligament is a completely extra-articular structure [124].



Fig. 49.33: Complete tear of the medial collateral ligament. Coronal T2-W MR image shows discontinuity (arrowhead) of the proximal portion of the medial collateral ligament with severe proximal stretching. The adjacent soft tissue shows diffuse swelling.

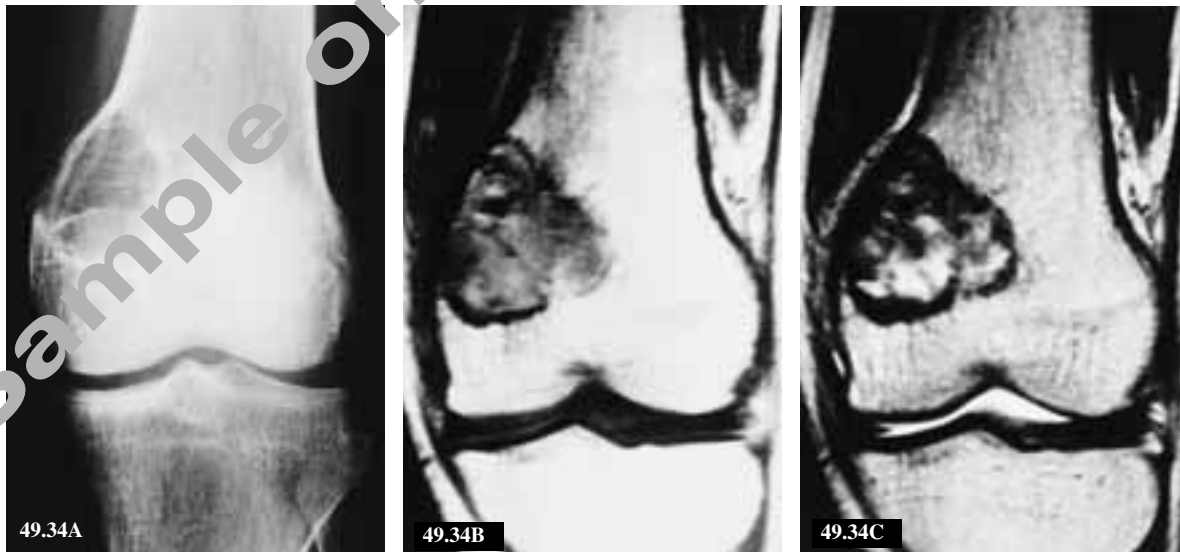


Fig. 49.34: Giant cell tumour of the distal femur. (A) AP radiograph of the knee shows a well-defined osteolytic lesion with cortical destruction and adjacent periosteal reaction of the distal femur. (B) Coronal T1-W MR image shows a predominantly-hypointense lesion at the distal metaphysis of the femur with partial involvement of the epiphysis. (C) Coronal T2-W MR image shows heterogeneous signal intensity of the lesion.

Tumours

Chondroblastoma is an uncommon primary cartilage tumour that occurs most frequently in the second and third decades of life. The typical radiographical appearance of chondroblastoma is a well-defined osteolytic lesion arising in the epiphysis or apophysis. The lesion has a thin sclerotic rim, with calcifications of the matrix. On MR imaging, chondroblastomas appear as well-defined, circumscribed hypointense regions on T1-weighted images and are hyperintense on T2-weighted images [125].

Giant cell tumour arises in the metaphysis, but almost invariably progress to contact the articular surface at the time of diagnosis. It is seen as a lytic lesion at the end of a long bone, with extensive contact with the articular surface, no matrix mineralisation, eccentric location, and a non-sclerotic margin. On MR imaging, giant cell tumour often shows intramural haemorrhage and cyst formation [126] (Fig. 49.34).

Osteosarcoma is the second most common primary malignant bone tumour, after myeloma. The tumour is often large at clinical presentation.

Radiographically, it may be predominantly osteosclerotic or osteolytic, but more frequently, it is of the mixed type. Radiographs characteristically reveal cloud-like densities representing tumour ossification. Bony destruction is usually of the moth-eaten or permeative type. Cortical bone is almost always destroyed in a disorderly fashion. A coexistent soft tissue mass is usually present, and is a major sign of malignancy [127] (Fig. 49.35).

Infection

Early detection of osteomyelitis and soft tissue infection is essential to ensure appropriate therapy and optimal clinical outcome. Osteomyelitis may be due to haematogeneous or contiguous infection. Haematogeneous osteomyelitis most often involves rapidly-growing bone, characteristically the metaphyses of the long bones in children, such as the distal femur or proximal tibia. The earliest radiographical features of acute haematogenous osteomyelitis are due to soft tissue changes. Swelling of the deep soft tissues adjacent to the involved bone develops 2 days to 3 days after the onset of acute haematogenous osteomyelitis. Bone changes are not usually

evident for the first 10 days to 14 days, or until 35% to 50% of the bone has been destroyed. Bone and periosteal abnormalities vary with the patient's age, the type of bone involved, and the infecting organism. Epiphyseal involvement results in more frequent extension into the joint space. Periosteal changes are less obvious because the periosteum is more firmly attached to bone in adults, compared to infants and children. Progression into cortical and periosteal tissues can lead to soft tissue abscess and fistula formation [128].

Tuberculous osteomyelitis may involve patients in all age ranges, but it is rare in infants. Bone and joint involvement occurs in 3% to 5% of patients with tuberculosis. When present, the disease usually presents with haematogenous dissemination to the metaphyseal region of long bones in children, and to the epiphyseal region in adults. Tuberculous

osteomyelitis may be difficult to differentiate from acute pyogenic osteomyelitis and fungal infection. However, tuberculosis and fungal disease tend to have a more subtle course, requiring more time for bone and joint changes to occur. With pyogenic infection, the course is much more rapid and joint involvement is less common than with tuberculosis [128].

Infective arthritis most commonly involves the larger joints (hip and knee). Monoarticular involvement is common, a finding that is useful in differentiating this entity from other arthropathies that are more commonly polyarticular or bilateral. The earliest radiographical findings involve the soft tissues. Periarticular swelling and effusions are most easily detected on the lateral radiograph. Destructive changes in articular cartilage begin early with pyogenic infection. If the diagnosis is



Fig. 49.35: Osteosarcoma of the distal femur. (A) Coronal T1-W MR image shows a diffuse hypointense lesion at the metaphysis of the femur with cortical destruction. The periosteum is displaced, and an extraosseous mass is noted at the medial aspect of the periosteum. (B) Coronal T2-W MR image shows a diffuse hyperintense lesion with a central hypointense portion.

delayed, joint infections can progress to involve the bones on either side of the joint. Further progression may result in fibrous or bony ankylosis, and growth disturbances in children [129].

Miscellaneous lesions

Osteochondritis dissecans

Osteochondritis dissecans refer to chondral and subchondral fragmentation of a portion of the articular surface. Boys are affected with greater frequency than girls, and the right knee is involved slightly more often than the left. Radiographs are sensitive in detecting most osteochondral lesions, but are not accurate in staging the lesions for therapeutic purposes. In addition to detecting the bony lesion, MR imaging can detect the presence of fluid or bone marrow oedema adjacent to the

osteochondral fragment, thus providing a clue to the stability of the lesion which is essential in selecting surgical versus conservative management [130] (Fig. 49.36).

Avascular necrosis

The medial femoral condyle is the most common site of involvement, although patients with predisposing conditions for AVN in general (e.g. corticosteroid therapy, organ transplantation, lupus erythematosus) frequently have lateral condylar or bicompartiment disease. Radiographical findings may initially be normal. With persistent symptoms, subcondylar flattening and sclerosis occur in the nature course of the disease. Finally, progression to collapse of the subchondral plate is observed [131] (Fig. 49.37).



Fig. 49.36: Osteochondritis dissecans of the medial femoral condyle. (A) Coronal PD-W MR image shows a button-shaped hypointense fragment (arrow) at the medial femoral condyle. (B) Sagittal PD-W MR image shows a fragment (arrow) and marginal sclerosis (arrowheads) at the medial femoral condyle.

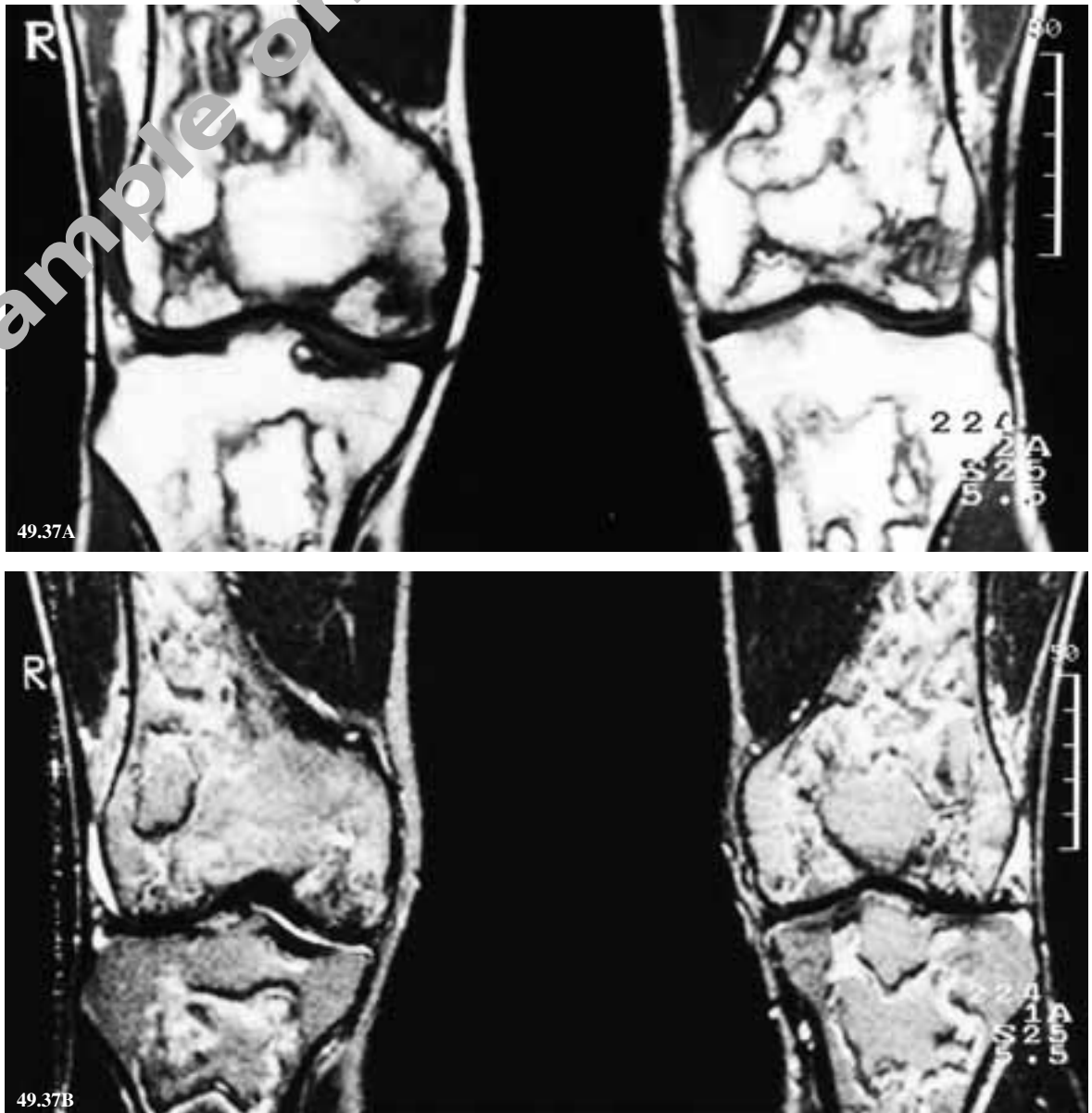


Fig. 49.37: Avascular necrosis of the femur and the tibia. Coronal (A) T1-W and (B) T2-W MR images show geographical lesions with hypointense rims at the distal femur and the proximal tibia. On T2-W images, band-like hyperintense rims are seen along the inner margins of the lesions.

Ganglion

In the knee, the most common site of ganglion formation is adjacent to a cruciate ligament. On MR images, ganglia appear as well-defined fluid collections, often with prominent septations [132].

Baker cyst

Baker cyst represents extrusion of joint fluid

through a weak portion of the joint capsule into the gastrocnemius-semimembranosus bursa. A constant anatomical feature of Baker cyst is that the cyst always extends between the semimembranosus tendon and the tendon of the medial head of the gastrocnemius muscle. On MR images, a Baker cyst appears as a well-defined lesion arising from the posteromedial aspect of the knee joint, with



Fig. 49.38: Synovial osteochondromatosis of the knee. (A) Sagittal T2-W and (B) coronal T2-W MR images show hypointense bodies (arrowheads) in the fluid-filled suprapatellar bursa.

hypointense signal on T1-weighted images and hyperintense signal on T2-weighted images [132].

Synovial osteochondromatosis

Synovial osteochondromatosis is due to chondroid metaplasia of the synovial membrane of joints, bursae, and tendon sheaths. On MR imaging, synovial osteochondromatosis usually appears as multiple intra-articular bodies surrounded by a joint effusion [133]. Immature cartilaginous fragments are hypointense on T1-weighted images and hyperintense on T2-weighted images. Calcification of the chondroma produces a hypointense rim on all pulse sequences (Fig. 49.38).

ANKLE

The ankle joint is considered to be a hinge joint. One may best understand the anatomy of the ankle by thinking in sets of three: three bones and three

important sets of ligaments. The three bones, i.e. the distal tibia, distal fibula, and talus, are held together by a series of three ligamentous complexes [134]. The ankle joint is surrounded by an articular capsule that is attached to the borders of the articular surfaces of the malleoli proximally, and to the talus on its articular surface distally. Radiographical evaluation of ankle and foot injuries is complicated by the presence of multiple accessory ossicles, which are considered secondary centres of ossification, and the sesamoid bones, all of which may mimic fractures.

Fractures and dislocations

These may be classified, according to the mechanism of injury, into inversion or eversion injuries. These broad categories represent a spectrum ranging from mild ligamentous injury to severe fracture and dislocation. Fractures of the ankle may also be clas-

sified by the anatomical structures involved, namely: single malleolus, bimalleolar (medial and lateral malleoli), or trimalleolar (medial, lateral, and posterior malleoli) fracture (Fig. 49.39). Complex fractures have also been described [134].

Fractures of the distal tibia

A fracture of the distal tibia is called a **pylon fracture** when the fracture line extends into the subtalar joint. There is severe distal tibial comminution along the tibial plafond. The malleoli maintain their normal anatomical position. Associated fractures of the medial and lateral malleoli are common and fractures of the talus are not uncommon. All of these injuries result from axial compression of the ankle joint, with or without rotary components [135].

Tillaux fracture describes an ankle fracture resulting from an abduction and external rotation

injury, and consists of avulsion of the lateral margin of the tibia. In adults, the radiographical appearance is typical, with a vertical fracture line in the posterolateral aspect of the tibia, extending from the articular surface up to the point of the fused epiphyseal plate [134]. In children, the so-called juvenile Tillaux fracture is actually a Salter-Harris type III injury to the growth plate.

Triplane fracture (Marmor-Lynn) is a fracture involving the lateral aspect of the distal tibial epiphysis. It may be complicated by extension of the fracture line into two other planes, hence the term triplane fracture. The mechanism of this type of injury is usually plantar flexion and external rotation [136].

Fractures of the fibula

Pott fracture usually occurs as a result of disruption of the tibiofibular syndesmosis.



Fig. 49.39: Trimalleolar fractures. (A) AP and (B) lateral radiographs show fractures of medial, lateral, and posterior malleoli.

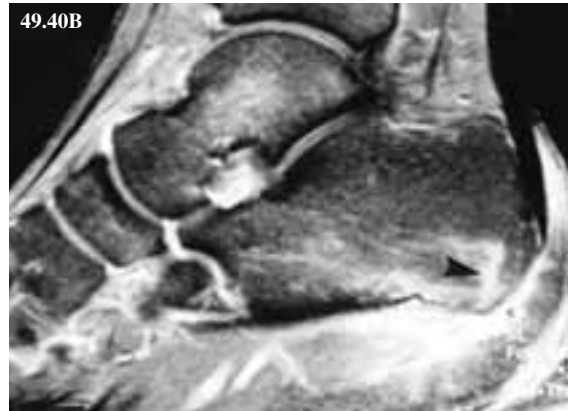
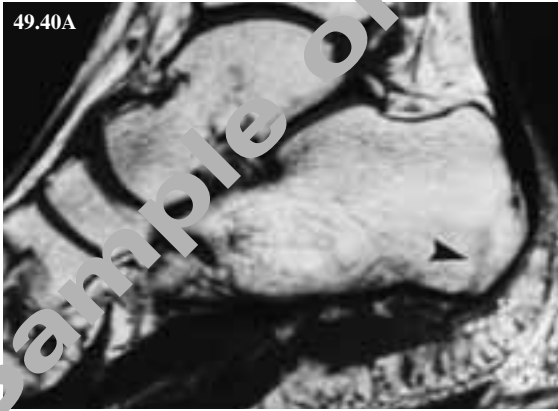


Fig. 49.40: Stress fracture of the calcaneum. (A) Sagittal T1-W MR image shows an area of band-like hypointense signal at the posteroinferior portion of the calcaneum. (B) Enhanced sagittal fat-suppressed T1-W MR image shows a corresponding area of band-like hyperintense signal.

Dupuytren fracture is a fracture of the fibula occurring 2 cm to 7 cm above the distal tibiofibular syndesmosis, and includes disruption of the medial collateral ligament. **Maisonneuve fracture** is an eversion-type injury of the fibula. The fracture, however, occurs in the proximal half of the bone, commonly at the junction of the proximal and middle thirds of the shaft. The tibiofibular syndesmosis is disrupted, and either tear of the tibiofibular ligament or fracture of the medial malleolus is also present.

Calcaneal stress fracture

Calcaneal stress fracture, like stress fractures elsewhere in the body, represents a partial or complete fracture of bone due to chronic repetitive trauma. Radiographs are most commonly normal on initial presentation. After several weeks, radiographs may show a vertical sclerotic band running from the posterosuperior plateau into the cancellous part of the calcaneus, perpendicular to the trabecular pattern. MR imaging identifies stress fractures as band-like areas of hypointense signal in the intramedullary space, usually extending to the cortex. A larger surrounding area of oedema and haemorrhage has a hypointense signal on T1-weighted images which becomes isointense or hyperintense to marrow fat on T2-weighted images

[137] (Fig. 49.40).

Soft tissue injuries and lesions

Injuries of ankle ligaments

Localisation of the ligamentous injury is currently based on the largely subjective or indirect findings of the history of the injury, physical examination, stress radiographs, and arthrography. Knowledge of the pertinent anatomy of the important ligaments of the ankle, especially their orientation, and the specific positioning of the foot or the proper imaging plane for their optimal visualisation, are important [138]. Diagnosis of ligament disruption usually requires special studies. Routine ankle radiographs are not usually effective in differentiating the types of ankle sprains.

The anterior and posterior tibiofibular ligaments are flat, four-sided ligaments that descend slightly from their tibial to their fibular attachments. On MR imaging, axial images that are obtained within 1 cm of the tibial plafond provide the best visualisation of these ligaments. The inferior tibiofibular ligament is located just below the posterior tibiofibular ligament. With the rupture of ligaments binding the distal tibia to the fibula, the medial malleolus is often fractured. There may also be rupture of the deltoid ligament, allowing the talus to move laterally and push the fibula away from the tibia.

The three lateral collateral ligaments each have an obliquity that requires careful foot positioning to obtain the optimum axial images. The anterior fibulotalar ligament is part of a quadrilateral ligament within the joint capsule. It courses from the anterior margin of the lateral malleolus to a talar attachment just anterior to its fibular articular surface. The posterior fibulotalar ligament extends medially from the deep aspect of the lateral malleolus to achieve an extensive mediolateral attachment to the talus. The fibulocalcaneal ligament arises from the deep aspect of the fibular malleolus. The ligament courses substantially downwards and backwards to its attachment at the lateral aspect of the calcaneus. Acute or subacute injury to any of the lateral collateral ligaments is invariably associated with considerable joint effusion, which in turn serves to provide contrast within the joint that greatly assists the diagnosis of the ligamentous injuries.

sis of the ligamentous injuries.

The medial collateral or deltoid ligament is delta-shaped, with an apical attachment above to the medial malleolus. It has a broad base below that attaches to the talus, the navicular and spring ligaments, and the calcaneus. The deltoid ligament is composed of superficial and deep layers. The bands of the superficial layer are relatively vertically orientated, originating from the tip of the medial malleolus and descending to attach, from anterior to posterior, to the navicular bone, spring ligament, and calcaneum. The superficial layer contains tibionavicular, tibiospring, and tibiocalcaneal components. The deep layer attaches to the medial aspect of the talus from its posterior process to its neck, and separates the ankle and subtalar joints. The thickest and strongest element of the deltoid ligament is the posterior tibiotalar portion of the deep deltoid, which

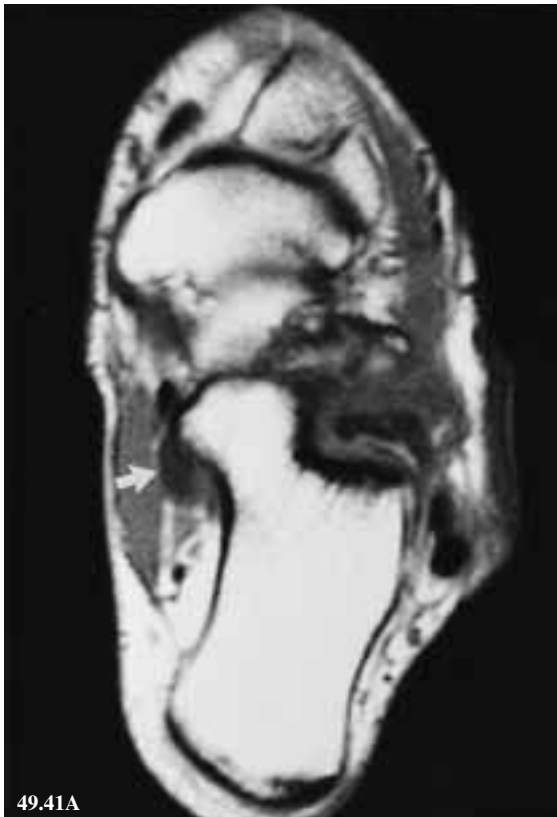


Fig. 49.41: Tarsal tunnel syndrome caused by a ganglion. (A) Axial T1-W MR image shows a small hypointense lesion (arrow) at the medial aspect of the sustentaculum tali. (B) Axial T2-W MR image shows a hyperintense lesion (arrow) representing the ganglion.

courses relatively transversely to attach to a large area on the posterior talar body.

The spring (plantar calcaneonavicular) ligament extends from the sustentaculum tali to the plantar aspect of the navicular. It is the major support for the talar head. It is therefore a major support for the longitudinal arch of the foot. This ligament is thick and very strong. Therefore, it practically never ruptures with the usual injuries of the ankle.

Tarsal tunnel syndrome

Several nerve compression syndromes have been reported in the foot. The most common of these is the tarsal tunnel syndrome, which is a symptom-complex characterised by pain or paraesthesia along the plantar aspect of the foot and toes. The tarsal tunnel is a fibro-osseous tunnel that extends from the level of the medial malleolus to the level of the tarsal navicular. It occupies the medial posterior aspect of the ankle, and extends into the medial plantar aspect of the foot. Tarsal tunnel syndrome may occur whenever the contents of the tunnel are compressed either intrinsically or extrinsically. Among the many lesions that have been described are ganglion, varicosity, lipoma, neurilemmoma, neurofibroma, synovial sarcoma, tenosynovitis of the flexor tendon, fibrosis following fracture, and synovial hypertrophy from rheumatoid arthritis [139] (Fig. 49.41).

Sinus tarsi syndrome

Sinus tarsi syndrome is due to pathological processes in the tarsal canal and sinus. Most patients present with history of ankle sprain or inversion injury. Characteristically, the patient has lateral ankle or hindfoot pain with point tenderness to palpation or pressure over the tarsal sinus [140]. The sinus tarsi is an anatomical space located between the inferior aspect of the talus and the superior aspect of the calcaneum, just anterior to the posterior subtalar joint. The osseous walls of the sinus

tarsi are irregular and are covered by multiple vascular foramina. The entire space is filled with fat and ligamentous structures. The main ligament occupying the sinus tarsi is the talocalcaneal or interosseous ligament which is broad and very strong. The most frequent cause of the sinus tarsi syndrome is trauma (70%). Inflammatory conditions and foot deformities constitute the remaining 30% of reported cases.

Plantar fasciitis

Plantar fasciitis is a painful condition with debilitating results. The plantar fascia, also described as the plantar aponeurosis, is a multilayered fibrous aponeurosis. It is comprised of three distinct components located medially, centrally, and laterally. The term plantar fasciitis is applied most frequently to a clinical presentation of pain and tenderness originating at the anteromedial surface of the calcaneal tuberosity. MR imaging is specific for diagnosis of fascial inflammation, and partial or complete rupture. T2-weighted sequences obtained in the sagittal, axial and coronal planes are most useful to measure the fascia, and to detect inflammatory changes or tears. These changes are seen as areas of increased signal intensity contrasted with the normal hypointense plantar fascia [141].

Achilles tendon

The Achilles tendon is the largest and strongest tendon in the foot and ankle. The tendon originates as the gastrocnemius and soleus tendons unite, and inserts on the posterior calcaneum. This tendon is typically approximately 8 cm long, and usually less than 1 cm in anteroposterior thickness. It can measure up to 1.5 cm in medial-lateral dimension. The normal Achilles tendon appears on MR imaging as a long, thin area of homogeneous hypointensity on sagittal images. Acute complete ruptures of the Achilles tendon are routinely and confidently diagnosed by MR imaging as complete disruption of the

tendon fibres, with fraying or retraction of the tendon ends. In cases of partial tendon ruptures, the disruption is not complete and some fibres may be seen in continuity [14].

Bursitis

The heel has two bursae. The retrocalcaneal bursa is located between the calcaneum and Achilles tendon, while the subcutaneous bursa is superficial to the tendon. Retrocalcaneal bursitis represents inflammation of the bursa that arises most commonly from overuse but also may develop in systemic disorders such as rheumatoid arthritis and seronegative spondyloarthropathies. MR imaging may be diagnostic, demonstrating a well-circumscribed region with signal characteristics of fluid in the anatomical location of the bursa [137].

REFERENCES

1. Resnick D, Kang HS. Shoulder. In: Resnick D, Kang HS, eds. *Internal Derangements of Joints: Emphasis on MR Imaging*. Philadelphia: WB Saunders, 1997: 163-333.
2. Neer CS. Anterior acromioplasty for the chronic impingement syndrome in the shoulder. *J Bone Joint Surg* 1972; 54A:41-50.
3. Tirman PFJ, Steinbach LS, Bezler JP, Bost FW. A practical approach to imaging of the shoulder with emphasis on MR imaging. *Orthop Clin North Am* 1997; 28:483-515.
4. Kieft GJ, Bloem JL, Rozing PM, Obermann WR. Rotator cuff impingement syndrome: MR imaging. *Radiology* 1988; 166:211-214.
5. Seeger LL, Gold RH, Bassett LW, Ellman H. Shoulder impingement syndrome: MR findings in 53 shoulders. *Am J Roentgenol* 1988; 150:343-347.
6. Farley TE, Neumann CH, Steinbach LS, et al. The coracoacromial arch: MR evaluation and correlation with rotator cuff pathology. *Skeletal Radiol* 1994; 23:641-645.
7. Needell SD, Zlatkin MB, Sher JS, et al. MR imaging of the rotator cuff: peritendinous and bone abnormalities in an asymptomatic population. *Am J Roentgenol* 1996; 166:863-867.
8. Burns WC, Whipple TL. Anatomic relationships in the shoulder impingement syndrome. *Clin Orthop* 1993; 294:96-102.
9. Seeger LL. Magnetic resonance imaging of the shoulder. In: Seeger LL, ed. *Diagnostic Imaging of the Shoulder*. Baltimore: Williams & Wilkins, 1992: 119-139.
10. Neumann CH, Holt RG, Steinbach LS, et al. MR imaging of the shoulder: appearance of the supraspinatus tendon in asymptomatic volunteers. *Am J Roentgenol* 1992; 158:1281-1287.
11. Farley TE, Neumann CH, Steinbach LS, et al. Full-thickness tears of the rotator cuff of the shoulder: diagnosis with MR imaging. *Am J Roentgenol* 1992; 158:347-351.
12. Kjellin I, Ho CP, Cervilla V, et al. Alterations in the supraspinatus tendon at MR imaging: correlation with histopathologic findings in cadavers. *Radiology* 1991; 181:837-841.
13. Rafii M, Firooznia H, Sherman O, et al. Rotator cuff lesions: signal patterns at MR imaging. *Radiology* 1990; 177:817-823.
14. Burk DL Jr, Karasick D, Mitchell DG, et al. MR imaging of the shoulder: correlation with plain radiography. *Am J Roentgenol* 1990; 154:549-553.
15. Griffith JF, Peh WCG, Evans NS, et al. Multiple rice body formation in chronic subacromial/subdeltoid bursitis: MR appearances. *Clin Radiol* 1996; 51:511-514.
16. Fritz RC, Helms CA, Steinbach LS, et al. Subscapular nerve entrapment: evaluation with MR imaging. *Radiology* 1992; 182:437-444.
17. Field LD, Altchek DW. Elbow injuries. *Clin Sports Med* 1995; 14:59-78.
18. Patten RM. Overuse syndromes and injuries involving the elbow: MR imaging findings. *Am J Roentgenol* 1995; 164:1205-1211.
19. Schenk M, Dalinka MK. Imaging of the elbow—an update. *Orthop Clin North Am* 1997; 28:517-535.
20. Fritz RC, Steinbach LS, Tirman PFJ, Martinez S. MR imaging of the elbow: an update. *Radiol Clin North Am* 1997; 35:117-144.
21. Bouffard A, Cho KH, Cardinal E, Chhem RK. Elbow. In: Cardinal E, Chhem RK, eds. *Guidelines and Gamuts in Musculoskeletal Ultrasound*. Wiley-Liss, 1999: 73-105.
22. Chhem RK, Cardinal E, Cho KH. Skeletal and superficial soft tissues. In: McGahan, Goldberg B, eds. *Diagnostic Ultrasound: a Logical Approach*. Philadelphia: Lippincott-Raven, 1998: 1115-1134.
23. Leach RE, Miller JK. Lateral and medial epicondylitis of the elbow. *Clin Sports Med* 1987; 6:259-272.
24. Potter HG, Hannafin JA, Morwessel RM, et al. Lateral epicondylitis: correlation of MR imaging, surgical, and histopathologic findings. *Radiology* 1995; 196:43-46.
25. Regan W, Wold LE, Coonrad R, et al. Microscopic histopathology of chronic refractory lateral epicondylitis. *Am J Sports Med* 1992; 20:746-749.
26. Nirschl RP. Sports and overuse injuries to the elbow. In: Morrey BF, ed. *The Elbow and Its Disorders*. Philadelphia: WB Saunders, 1985: 309-341.
27. Maffulli N, Regine R, Carrillo F, et al. Tennis elbow: an ultrasonographic study in tennis players. *Br J Sports Med* 1990; 24:151-155.
28. Ho CH. Sports and occupational injuries of the elbow: MR imaging findings. *Am J Roentgenol* 1995; 164:1465-1471.
29. Sonin AH, Tutton SM, Fitzgerald SW, Peduto AJ. MR imaging of the adult elbow. *RadioGraphics* 1996; 16:1323-1336.
30. Falchok FS, Zlatkin MB, Erbacher GE, et al. Rupture of the distal biceps tendon: evaluation with MR imaging. *Radiology* 1994; 190: 659-663.
31. Loranzo V, Alonso P. Sonographic detection of the distal biceps tendon rupture. *J Ultrasound Med* 1995; 14:389-391.
32. Kaempffe FA, Lerner RM. Ultrasound diagnosis of triceps tendon rupture. *Clin Orthop* 1996; 332:138-142.

33. Schweitzer M, Morrison WB. Arthroplasties and inflammatory conditions of the elbow. *MRI Clin North Am* 1997; 5:603-617.
34. Liessi G, Cesari S, Spaliviero B, et al. The US, CT, and MRI findings of cubital bursitis: a report of five cases. *Skeletal Radiol* 1996; 25:471-475.
35. Skaf AY, Boutin R, Dantas RWM, et al. Bicipitoradial bursitis: MR imaging findings in 8 patients and anatomic data from contrast material opacification of bursae followed by routine radiography and MR imaging in cadavers. *Radiology* 1999; 212:111-116.
36. Rosenberg ZS, Beltran J, Cheung YY, et al. The elbow: MR features of nerve disorders. *Radiology* 1993; 188: 235-240.
37. Beltran J, Rosenberg ZS. Diagnosis of compressive and entrapment neuropathies of the upper extremity: value of MR imaging. *Am J Roentgenol* 1994; 163:525-531.
38. Martinoli C, Bianchi S, Derchi LE. Tendon and nerve sonography. *Radiol Clin North Am* 1999; 37: 691-711.
39. Butters KP, Morrey BF. Septic arthritis. In: Morrey BF, ed. *The Elbow and Its Disorders*. 2nd ed. Philadelphia: WB Saunders, 1993: 784-791.
40. Lim-Dunham JE, Ben-Ami TE, Yousefzadeh DK. Septic arthritis of the elbow in children: the role of sonography. *Pediatr Radiol* 1995; 25:556-559.
41. Wang SC, Chhem RK, Cardinal E, Cho KH. Joint sonography. *Radiol Clin North Am* 1999; 37:653-668.
42. Frankel DA, Bargiela A, Bouffard JA, et al. Synovial joints: evaluation of intraarticular bodies with US. *Radiology* 1998; 206:41-44.
43. Bianchi S, Martinoli C. Detection of loose bodies in joints. *Radiol Clin North Am* 1999; 37:679-690.
44. Quinn SF, Haverman JJ, Fitzgerald SW, et al. Evaluation of loose bodies in the elbow with MR imaging. *J Magn Reson Imaging* 1994; 4:169-172.
45. Fritz RC. MR imaging of osteochondral and articular lesions. *MRI Clin North Am* 1997; 5:579-602.
46. Peiss J, Adam G, Casser R, et al. Gadopentetate-dimeglumine-enhanced MR imaging of osteonecrosis and osteochondritis dissecans of the elbow: initial experience. *Skeletal Radiol* 1995; 24:17-20.
47. Rosenberg ZS, Beltran J, Cheung YY. Pseudodeflect of the capitellum: potential MR imaging pitfall. *Radiology* 1994; 191:821-823.
48. Kransdorf MJ. Benign soft-tissue tumors in a large referral population: distribution of specific diagnosis by age, sex, and location. *Am J Roentgenol* 1995; 164:395-402.
49. Kransdorf MJ. Malignant soft-tissue tumors in a large referral population: distribution of specific diagnosis by age, sex, and location. *Am J Roentgenol* 1995; 164:129-134.
50. Fornage BD. Soft-tissue masses. In: Fornage BD, ed. *Musculoskeletal Ultrasound*. New York: Churchill-Livingstone, 1995; 21-42.
51. Ceulemans R, van Holsbeeck M. Ultrasonography: In: De Schepper AM, ed. *Imaging of Soft Tissue Tumors*. Berlin: Springer-Verlag, 1997: 3-18.
52. Van der Woude H, Vanderschueren G. Ultrasound in musculoskeletal tumors with emphasis on its role in tumor follow-up. *Radiol Clin North Am* 1999; 37:753-766.
53. Forrester DM, Brown JC. The ABC'S of the arthritis: the hand. In: Forrester DM, ed. *The Radiology of Joint Disease*. 3rd ed. Philadelphia: WB Saunders, 1987: 1-135.
54. Buckwalter KA, Shannon Swan J, Braunstein EM. Evaluation of joint disease in the adult hand and wrist. *Hand Clinics* 1991; 7:135-151.
55. Yin Y, Mann FA, Gilula LA. Algorithmic approach to wrist pain. In: Gilula LA, Yin Y, eds. *Imaging of the Wrist and Hand*. Philadelphia: WB Saunders, 1996: 587-599.
56. Metz VM, Blum A, Bresler F, et al. Arthrography and CT-arthrography of the wrist and hand. In: Gilula LA, Yin Y, eds. *Imaging of the Wrist and Hand*. Philadelphia: WB Saunders, 1996: 367-400.
57. Lee D. Sonography of the wrist and hand. *Semin Musculoskeletal Radiol* 1998; 2:237-243.
58. Bianchi S, Martinoli C, Abdelwahab IF. High-frequency ultrasound examination of the wrist and hand. *Skeletal Radiol* 1999; 28:121-129.
59. Rettig ME, Raskin KB, Melone CP. Clinical applications of MR imaging in hand and wrist surgery. *MRI Clin North Am* 1995;3:361-368.
60. Chaisson CE, Zhang Y, McAlindon TE, et al. Radiographic hand osteoarthritis: incidence, patterns, and influence of pre-existing disease in a population based sample. *J Rheumatol* 1997; 24:1337-1343.
61. Bullough PG, Bansal M. The differential diagnosis of geodes. *Radiol Clin North Am* 1988; 26:1165-1184.
62. Bergman AG. Synovial lesions of the hand and wrist. *MRI Clin North Am* 1995; 3:265-279.
63. Martel W, Hayes JT, Duff IF. The pattern of bone erosion in the hand and wrist in rheumatoid arthritis. *Radiology* 1965; 84:206.
64. Renner WR, Weinstein AS. Early changes of rheumatoid arthritis in the hand and wrist. *Radiol Clin North Am* 1988; 26:1185-1193.
65. Sugimoto H, Takeda A, Masuyama J, et al. Early rheumatoid arthritis: diagnostic accuracy of MR imaging. *Radiology* 1996; 198:185-192.
66. Backhaus M, Kamradt T, Sandrock D, et al. Arthritis of the finger joints: a comprehensive approach comparing conventional radiography, scintigraphy, ultrasound, and contrast-enhanced MR imaging. *Arthritis Rheum* 1999; 42:1232-1245.
67. Lund PJ, Heikal A, Maricic MJ, et al. Ultrasonographic imaging of the hand and wrist in rheumatoid arthritis. *Skeletal Radiol* 1995; 24:591-596.
68. Golimbu CN, Firooznia H, Rafii M. Avascular necrosis of carpal bones. *MRI Clin North Am* 1995; 3:281-303.
69. Totterman SMS, Miller RJ. MR imaging of the triangular fibrocartilage complex. *MRI Clin North Am* 1995; 3:213-228.
70. Zlatkin MB, Chao PC, Osterman AL, et al. Chronic wrist pain: evaluation with high-resolution MR imaging. *Radiology* 1989; 173:723-729.
71. Oneson SR, Timins ME, Scales LM, et al. MR imaging diagnosis of triangular fibrocartilage pathology with arthroscopic correlation. *Am J Roentgenol* 1997; 168:1513-1518.
72. Totterman SMS, Miller RJ, McCance SE, et al. Lesions of the triangular fibrocartilage complex: MR findings with a three-dimensional gradient-recalled echo sequence. *Radiology* 1996; 199:227-232.
73. Yin Y, Mann FA, Hodge JC, Gilula LA. Roengenographic interpretation of ligamentous instabilities of the wrist. In: Gilula LA, Yin Y, eds. *Imaging of the Wrist and Hand*.

- Philadelphia: WB Saunders, 1996; 203-224.
74. Mann FA, Wilson AJ, Gilula LA. Radiographic evaluation of the wrist: What does the hand surgeon want to know? *Radiology* 1992; 184:15-24.
 75. Smith DK. MR imaging of normal and injured wrist ligaments. *MRI Clin North Am* 1995; 3:229-248.
 76. Totterman SM, Miller RJ, Wasserman B, et al. Intrinsic and extrinsic carpal ligaments: evaluation by three-dimensional Fourier transform MR imaging. *Am J Roentgenol* 1995; 160:117-123.
 77. Weinstein AJ, Koniuch MP, van Holsbeeck M. Ultrasonographic detection of thumb ulnar collateral ligament injuries: a cadaveric study. *J Hand Surg* 1994; 19A:304-312.
 78. Spaeth HJ, Abrams RA, Bock GW, et al. Gamekeeper thumb: differentiation of nondisplaced and displaced tears of the ulnar collateral ligament with MR imaging. *Radiology* 1993; 188: 553-556.
 79. Noszian IM, Dinkhauser LM, Orthner E, et al. Ulnar collateral ligament: differentiation of nondisplaced and displaced tears with ultrasound. *Radiology* 1995; 194:61-63.
 80. Hergan K, Mittler C, Oser W. Ulnar collateral ligament: differentiation of nondisplaced and displaced tears with ultrasound and MR imaging. *Radiology* 1995; 194:65-71.
 81. Read JW, Conolly WB, Lanzetta M, et al. Diagnostic ultrasound of the hand and wrist. *J Hand Surg* 1996; 21A:1004-1010.
 82. Rubin DA, Kneeland JB, Kitay GS, et al. Flexor tendon tears in the hand: use of MR imaging to diagnose degree of injury in a cadaver model. *Radiology* 1996; 166:615-620.
 83. De Flaviis L, Musso MG. Hand and wrist. In: Fornage BD, ed. *Musculoskeletal Ultrasound*, New York: Churchill-Livingstone, 1995: 151-178.
 84. Serafini G, Derchi LE, Quadri P, et al. High resolution sonography of the flexor tendon in trigger fingers. *J Ultrasound Med* 1996; 16:213-219.
 85. Giovagnorio F, Andreoli C, De Cicco ML. Ultrasonographic evaluation of de Quervain disease. *J Ultrasound Med* 1997; 16:685-689.
 86. Klug JD. MR diagnosis of tenosynovitis about the wrist. *MRI Clin North Am* 1995;3:305-312.
 87. Jelinek JS, Kransdorf MJ, Shmookler BM, et al. Giant cell tumor of the tendon sheath: MR findings in nine cases. *Am J Roentgenol* 1994; 162:919-922.
 88. Lee D, van Holsbeeck M, Janevski PK, et al. Diagnosis of carpal tunnel syndrome: ultrasound vs. electromyography. *Radiol Clin North Am* 1999; 37:859-872.
 89. Mesgarzadeh M, Triolo J, Schneck CD. Carpal tunnel syndrome: MR imaging diagnosis. *MRI Clin North Am* 1995; 3:249-264.
 90. Kransdorf MJ, Murphey MD. MR imaging of musculoskeletal tumors of the hand and wrist. *MRI Clin North Am* 1995; 3:327-344.
 91. Fornage BD, Schernberg FL, Rifkin MD. Ultrasound examination of the hand. *Radiology* 1985; 155:785-788.
 92. Peh WCG, Truong NP, Totty WG, Gilula LA. Magnetic resonance imaging of benign soft tissue masses of the hand and wrist. *Clin Radiol* 1995; 50:519-525.
 93. Fornage BD. Glomus tumors in the fingers: diagnosis with US. *Radiology* 1988; 167:183-185.
 94. Drape JL, Idy-Peretti I, Goettmann S, et al. Subungual glomus tumors: evaluation with MR imaging. *Radiology* 1995; 195:507-515.
 95. Resnick D, Kang HS. Pelvis and hip. In: Resnick D, Kang HS, eds. *Internal Derangements of Joints: Emphasis on MR Imaging*. Philadelphia: WB Saunders, 1997: 473-554.
 96. Hayes CW, Balkisson ARA. Musculoskeletal imaging update, part I: current concepts in imaging of the pelvis and hip. *Orthop Clin North Am* 1997; 28:617-642.
 97. Ficat RP. Idiopathic bone necrosis of the femoral head: Early diagnosis and treatment. *J Bone Joint Surg* 1985; 67B:3-9.
 98. Mitchell DG, Rao VM, Dalinka MK, et al. Femoral head avascular necrosis: correlation of MR imaging, radiographic staging, radionuclide imaging, and clinical findings. *Radiology* 1987; 162:709-715.
 99. Van de Berg BE, Malgheem JJ, Labaisse MA, et al. MR imaging of avascular necrosis and transient marrow edema of the femoral head. *RadioGraphics* 1993; 13:501-520.
 100. Guerra J, Steinberg M. Distinguishing transient osteoporosis from avascular necrosis of the hip. *J Bone Joint Surg* 1995; 77A:616-624.
 101. Major NM, Helms CA. Idiopathic transient osteoporosis of the hip. *Arthritis Rheum* 1997; 40:1178-1179.
 102. Fairclough J, Colhoun E, Johnston D, et al. Bone scanning for suspected hip fractures: a prospective study in elderly patients. *J Bone Joint Surg* 1987; 69B:251- 253.
 103. Deutsch AL, Mink JH, Waxman AD. Occult fractures of the proximal femur: MR imaging. *Radiology* 1989; 170:113-116.
 104. Gerscovich EO. A radiologist's guide to the imaging in the diagnosis and treatment of developmental dysplasia of the hip. I. General considerations, physical examination as applied to real-time sonography and radiography. *Skeletal Radiol* 1997; 26:386-397.
 105. Gerscovich EO. A radiologist's guide to the imaging in the diagnosis and treatment of developmental dysplasia of the hip. II. Ultrasonography: anatomy, technique, acetabular angle measurements, acetabular coverage of femoral head, acetabular cartilage thickness, three-dimensional technique, screening of newborns, study older children. *Skeletal Radiol* 1997; 26:447-456.
 106. Johnson ND, Wood BP, Jackman KV. Complex infantile and congenital hip dislocation: assessment with MR imaging. *Radiology* 1988; 168:151-156.
 107. Fisher R, O'Brien TS, Davis KM. Magnetic resonance imaging in congenital dysplasia of the hip. *J Pediatr Orthop* 1991; 11:617-622.
 108. Czerny C, Hofmann S, Neuhold A, et al. Lesions of the acetabular labrum: accuracy of MR imaging and MR arthrography in detection and staging. *Radiology* 1996; 200:225-230.
 109. Klauke K, Durnian CW, Ganz R. The acetabular rim syndrome: a clinical presentation of dysplasia of the hip. *J Bone Joint Surg* 1991; 73B:423-429.
 110. Fitzgerald RH. Acetabular labrum tears. *Clin Orthop* 1995; 311:60-68.
 111. Hodler J, Yu JS, Goodwin D, Haghighi P, Trudell D, Resnick D. MR arthrography of the hip: improved imaging of the acetabular labrum with histologic correlation. *Am J Roentgenol* 1995; 165:887-891.
 112. Petersilge CA, Haque MA, Petersilge WJ, Lewin JS,

- Lieberman JM, Buly R. Acetabular labral tears: evaluation with MR arthrography. *Radiology* 1996; 200:231-235.
113. Petersilge CA. Chronic adult hemipain: MR arthrography of the hip. *RadioGraphics* 2000; 20:43-52.
114. Edwards DJ, Lomas F, Guller RH. Diagnosis of the painful hip by magnetic resonance imaging and arthroscopy. *J Bone Joint Surg* 1995; 77B:374-376.
115. Hase T, Ueda T. Acetabular labral tear: arthroscopic diagnosis and treatment. *Arthroscopy* 1999; 15:138-141.
116. Haller J, Ganssler D, Greenway G, et al. Juxtaacetabular ganglionic (or synovial) cysts: CT and MR features. *J Comput Assist Tomogr* 1989; 13:976-983.
117. Greenspan A. *Orthopedic Radiology: A Practical Approach*. Philadelphia: JB Lippincott, 1988: 10.4-11.19.
118. Dorwart RH, Genant HK, Johnson WH, Morris JM. Pigmented villonodular synovitis of synovial joints-clinical, pathologic, and radiologic features. *Am J Roentgenol* 1984; 143:877-885.
119. Ryu KN, Jaovisidha S, Schweitzer M, Motta AO, Resnick D. MR imaging of lipoma arborescens of the knee joint. *Am J Roentgenol* 1996; 167:1229-1232.
120. Mink JH, Reicher MA, Crues JV, Deutsch AL. The menisci. In: Crues JV, Stoller DW, eds. *MRI of the Knee*. New York: Raven Press, 1993: 91-140.
121. Ryu KN, Kim IS, Kim EJ, et al. MR imaging of tears of discoid lateral menisci. *Am J Roentgenol* 1998; 171:963-967.
122. Burk DL, Dalinka MK, Kanal E, et al. Meniscal and ganglion cysts of the knee: MR evaluation. *Am J Roentgenol* 1988; 150:331-336.
123. Robertson PL, Schweitzer ME, Bartolozzi AR, Ugoni A. Anterior cruciate ligament tears: evaluation of multiple signs with MR imaging. *Radiology* 1994; 193:829-834.
124. Mink JH, Reicher MA, Crues JV, Deutsch AL. The cruciate and collateral ligaments. In: Mink JH, ed. *MRI of the Knee*. New York: Raven Press, 1993: 141-188.
125. Jee WH, Park YK, McCauley TR, et al. Chondroblastoma: MR characteristics with pathologic correlation. *J Comput Assist Tomogr* 1999; 23:721-726.
126. Manaster BJ, Doyle AJ. Giant cell tumors of bone. *Radiol Clin North Am* 1993; 31:299-323.
127. Bloem JL, Kroon HM. Osseous lesions. *Radiol Clin North Am* 1993; 31: 261-278.
128. Resnick D, ed. *Diagnosis of Bone and Joint Disorders*. 3rd ed. Philadelphia: WB Saunders, 1995.
129. Brower AC. Septic arthritis. *Radiol Clin North Am* 1996; 34:293-310.
130. Mesgarzadeh M, Sapega AA, Bonakdarpour A, et al. Osteochondritis dissecans: analysis of mechanical stability with radiography, scintigraphy, and MR imaging. *Radiology* 1987; 165:775-780.
131. Lotke P, Ecker ML. Osteonecrosis of the knee. *J Bone Joint Surg* 1988; 70A:470-473.
132. Janzen DL, Peterfy CG, Forbes JR, Tirman PFJ, Genant HK. Cystic lesions around the knee joint: MR imaging findings. *Am J Roentgenol* 1994; 163:155-161.
133. Tuckman G, Wirtz CZ. Synovial osteochondromatous of the shoulder: MR findings. *J Comput Assist Tomogr* 1989; 13: 360-361.
134. Daffner RH. Ankle trauma. *Radiol Clin North Am* 1990; 28:395-421.
135. Mainwaring BL, Daffner RH, Riemer BL. Pylon fracture of the ankle: a distinct clinical and radiologic entity. *Radiology* 1988; 168:215-218.
136. Greenspan A. *Orthopedic Radiology: A Practical Approach*. Philadelphia, JB Lippincott, 1988: 7.1-7.34.
137. Kier R, Dietz MJ, McCarthy SM, et al. MR appearance of painful conditions of the ankle. *RadioGraphics* 1991; 11:401-414.
138. Mesgarzadeh M, Schneck CD, Tehranzadeh J, Chandnani VP, Bonakdarpour A. Magnetic resonance imaging of ankle ligaments. *MRI Clin North Am* 1994; 2:39-58.
139. Finkel JE. Tarsal tunnel syndrome. *MRI Clin North Am* 1994; 2:67-78.
140. Klein MA, Spreitzer AM. MR imaging of the tarsal sinus and canal. Normal anatomy, pathologic findings, and features of sinus tarsi syndrome. *Radiology* 1993; 186:233-240.
141. Berkowitz JF, Kier R, Rudicel S. Plantar fasciitis: MR imaging. *Radiology* 1991; 179:665-667.
142. Quinn SF, Murray WT, Clark RA, et al. Achilles tendon: MR imaging at 1.5T. *Radiology* 1987; 164:767-770.